

COSMOLOGICAL INTERPRETATION OF THE COLOR-MAGNITUDE DIAGRAMS OF GALAXY CLUSTERS

MAURO SCIARRATTA,¹ CESARE CHIOSI,¹ MAURO D'ONOFRIO,^{1,2} AND STEFANO CARIDDI¹

¹*Department of Physics and Astronomy, Vicolo dell'Osservatorio, 3 I-35100 Padova, Italy*

²*INAF Observatory of Padova, Vicolo Osservatorio 5, I-35122 Padova, Italy*

(Received; Revised; Accepted)

Submitted to ApJ

ABSTRACT

We investigate the color-magnitude diagram (CMD) of cluster galaxies in the hierarchical Λ -CDM cosmological scenario using both single stellar populations and simple galaxy models. First, we analyze the effect of bursts and mergers and companion chemical pollution and rejuvenation of the stellar content on the integrated light emitted by galaxies. The dispersion of the galaxy magnitudes and colors on the $M_V - (B - V)$ plane is mainly due to mixing of ages and metallicities of the stellar populations, with mergers weighting more than bursts of similar mass fractions. The analysis is made using the Monte-Carlo technique applied to ideal model galaxies reduced to single stellar populations with galaxy-size mass to evaluate mass, age and metallicity of each object. We show that separately determining the contributions by bursts and mergers leads to a better understanding of observed properties of CMD of cluster galaxies. Then we repeat the analysis using suitable chemo-photometric models of galaxies whose mass is derived from the cosmological predictions of the galaxy content of typical clusters. Using the halo mass function and the Monte-Carlo technique, we derive the formation redshift of each galaxy and its photometric history. These are used to simulate the CMD of the cluster galaxies. The main conclusion is that most massive galaxies have acquired the red color they show today in very early epochs and remained the same ever since. The simulations nicely reproduce the Red Sequence, the Green Valley and the Blue Cloud, the three main regions of the CMD in which galaxies crowd.

Keywords: cosmology: large-scale structure of universe — galaxies: evolution — galaxies: photometry — galaxies: luminosity function, mass function — galaxies: starburst — methods: numerical

arXiv:1811.04605v1 [astro-ph.GA] 12 Nov 2018

1. INTRODUCTION

The color-magnitude diagram (CMD) is the reference diagnostic tool for understanding the physical properties of stars and stellar populations of any age, chemical composition and size going from simple star clusters to galaxies and on recent times the galaxy content of clusters of galaxies. Leaving aside the classical case of stars and star clusters, for which starting from the original studies by [Hertzsprung \(1909\)](#) and [Russell \(1914\)](#) nowadays there is an immense body of literature, and also those for our own Galaxy and galaxies in the Local Group and nearby Universe (e.g. [Andromeda Baade 1944](#); [Sandage 1957](#); [Blaauw 1959](#)), the CMD diagnostic has been extended to the integrated light of galaxies in clusters, e.g. like Virgo and Coma, to understand the physical properties of their galaxies (e.g. [Chester & Roberts 1964](#); [Chiosi 1967](#); [Visvanathan & Sandage 1977](#); [Sandage & Visvanathan 1978b,a](#)). The advent of modern instrumentation provided much richer CMDs ([Bower et al. 1992a](#); [Kodama et al. 1998, 1999](#); [Terlevich et al. 2001](#); [Bell et al. 2004](#), to mention a few) and allowed to infer information on the past history of the clusters themselves. Furthermore, since colors are independent on distance, for any cluster this latter is nearly the same for all member galaxies, and the fact that many (if not all) clusters do share many common features, their CMDs have been considered as key cosmological probes ([Tully et al. 1982](#); [Bower et al. 1992a](#)).

In this context, galaxy clusters play a key role in our understanding of not only galaxy formation and evolution but also the same cosmogony of the Universe. In brief, studies of nearby clusters have provided important informations about the gas content ([Davies & Lewis 1973](#); [Kennicutt 1983](#)), the very high mass-to-light ratios (several hundreds solar units) indicating large amounts of dark matter (DM; e.g. [Faber & Gallagher 1979](#); [Adami et al. 1998](#)), the gravitational lensing of distant objects in the Universe ([Bartelmann 2010](#), and references therein), the strong X-ray emission due to hot gas filling the intra-cluster medium (ICM; see e.g. [Gott & Gunn 1971](#); [Sunyaev & Zeldovich 1972](#)), the fractions of blue and red galaxies and their morphological ratios (both differ from the ones in the field [Butcher & Oemler 1978](#); [Dressler 1980](#)), the so-called galaxy color bi-modality ([Baldry et al. 2004](#)) and other issues not mentioned here. These features, together with phenomena like dynamical friction, tidal disruption, cooling flows and chemical enrichment of ICM from galactic winds, make clusters very similar objects: i.e. excellent tools for exploring the Universe ([Bower et al. 1992a](#)). Furthermore, several questions have been asked and answered in the past three decades thanks to galaxy clusters, e.g. cold DM as the concordance model to describe dynamical matter in the Universe and the non-hierarchical nature of baryonic

physics, together with the inherently famous problem of “downsizing” of galaxies (see [Kravtsov & Borgani 2012](#), for a detailed review, and all references therein for in-depth description of galaxy clusters). For all these reasons, the study of galaxy clusters and their galaxy content is of paramount importance.

As far as the CMDs are concerned, three main loci were soon identified: the first was the Red Sequence (firstly noted by [de Vaucouleurs 1961](#)), an almost perfectly linear band throughout a broad range of luminosities mainly occupied by evolved early-type galaxies. Since then thanks to many large scale surveys, magnitudes and colors in different photometric pass-bands, morphological types, redshifts, for hundreds of thousands of galaxies became available. To mention a few we recall the Galaxy Zoo from the Sloan Digital Sky Survey of [Blanton et al. \(2003\)](#), [Lintott et al. \(2008\)](#), [Wong et al. \(2012\)](#) so that the existence and evolution of the Red Sequence was widely confirmed ([Stott et al. 2009](#); [Head et al. 2014](#)), and more recently, the faint-end of this was also investigated (see [Boselli & Gavazzi 2014](#) for the faint-end of the Red Sequence in high density environments, [Roediger et al. 2017](#) for the faint-end of the Red Sequence in the Virgo clusters at the faintest magnitudes, and [Head et al. 2014](#) for dissecting the Red Sequence in bulge and disk of early-type galaxies in the Coma cluster). Finally, [Baldry et al. \(2004\)](#) quantified the bimodal CMDs of galaxies. Very soon it became evident that, in addition to the Red Sequence, two more regions in the CMDs are crowded by galaxies: the Blue Cloud, where gas-rich galaxies forming stars at high rates are found; the Green Valley, in between the first two, where a complicated interplay between gas conversion into new stars and the redward evolution of old stars is at work ([Menci et al. 2005](#)). All this is the analog of the bimodal color distribution of star clusters in the LMC ([Chiosi et al. 1988](#)), and globular clusters in our own and external galaxies (see [Cantiello & Blakeslee 2007](#), and references). In this context many attempts have been made to firmly define the three regions on the CMD. Unfortunately the task is difficult because of the well known age-metallicity degeneracy: stars and stellar populations become redder at increasing age and/or metallicity, to which in the case of galaxies at least one more cause must be added, i.e. the past star formation history of the system (see [Tinsley 1980](#) for a classical review of the basic concepts and the recent review by [Silk & Mamon 2012](#)).

Understanding the origin of the Red Sequence (otherwise named Color-Magnitude-Relation, CMR), its slope and width for the galaxies in the Local Universe has been the subject of many studies, among which we recall [Baum \(1959\)](#), [Faber \(1977\)](#), [Dressler \(1984\)](#), [Bower et al. \(1992a\)](#), [Burstein et al. \(1995\)](#), [Burstein et al. \(1997\)](#), [Gallazzi et al. \(2006\)](#), [Menci et al. \(2008\)](#), [Valentinuzzi et al. \(2011\)](#) to mention a few. In parallel, the galaxy CMR and its prop-

erties have the subject of intense observational and theoretical investigations among many others we recall Gladders et al. (1998), Tran et al. (2007), Mei et al. (2009). Basing on the classical scenario of galaxy formation and evolution in presence of supernova-driven galactic winds (Larson 1974; Arimoto & Yoshii 1987; Tantaló et al. 1996; Kodama & Arimoto 1997; Tantaló et al. 1998; Chiosi et al. 1998), on semi-analytical models in the hierarchical scheme (White & Frenk 1991; Kauffmann 1996; Kauffmann & Charlot 1998), and on NB-TSPH simulations of galaxy formation and evolution (e.g. Chiosi & Carraro 2002), the commonly accepted view emerged that the Red Sequence de facto is a metallicity sequence and not an age sequence, however with an age dispersion that seems to increase at decreasing galaxy mass. This conclusion requires an adequate treatment of the chemical evolution in the model galaxies to be taken into account, otherwise the slope of the CMR is not reproduced (Kauffmann 1996). This problem is persistent even in very recent studies (Nelson et al. 2018). Conversely, understanding the global appearance of the Red Sequence in the CMDs of cluster galaxies is still at its infancy (Menci et al. 2008; Lee et al. 2017, e.g.). This will be the main goal of our study.

In recent times, massive numerical large scale simulations of hierarchical galaxy formation in Λ -CDM cosmogony including both DM and baryonic matter (BM) have been made possible by the new generation of numerical codes developed by Hernquist & Springel (2003), Springel & Hernquist (2003a,b), Vogelsberger et al. (2012), Puchwein & Springel (2013), Barai et al. (2013) and references therein. In these, much effort is paid to include star formation and chemical enrichment, radiative cooling and heating in presence of an UV background radiation field, and feedback processes of different nature. With the aid of these simulations, the variation of the cosmic star formation rate density, SFRD(z), with redshift (see Madau & Dickinson 2014; Katsianis et al. 2017, and references) has been addressed and largely explained (Rasera & Teysier 2006; Hernquist & Springel 2003; Katsianis et al. 2017; Pillepich et al. 2017). In brief, they investigated the effect of the energy feedback from supernovae explosions, stellar winds, and AGN activity on modeling the cosmic star formation. They made use of an improved version of the code P-GADGET3 by Springel (2005) with chemical enrichment (Tornatore et al. 2007), supernova energy and momentum-driven galactic winds (Puchwein & Springel 2013), AGN feedback (Springel et al. 2005; Planelles et al. 2013), metal-line cooling (Wiersma et al. 2009b,a) plus molecules/metal cooling (Maio et al. 2007), supernova-driven galactic winds with feedback (Barai et al. 2013), thermal conduction (Dolag et al. 2004). Some of these simulations take also the photometric evolution of the stellar content of galaxies into account so that the CMDs are

possible, in particular for galaxies belonging to clusters, and consequently are used to prove the physical assumptions of the large scale cosmological simulations (see e.g. Nelson et al. 2015, 2018). Furthermore, theoretical studies (e.g. Bower et al. 2006; Henriques et al. 2015) are devoted to disentangling the effect of DM and BM on observable quantities: they have proven to be consistent with observations starting from a hierarchical point of view, even with increasing complexity of the underlying physics.

In the cosmological view of galaxy formation and evolution, steps forward have been made thanks to the halo mass functions (HMF), (e.g. Sheth & Tormen 2002; Warren et al. 2006; Tinker et al. 2008; Angulo et al. 2012; Behroozi et al. 2013), the integral of this over a given mass interval, named the halo growth function (HGF), (Lukić et al. 2007), and merger trees (e.g. Boylan-Kolchin et al. 2009; Guo et al. 2011) calculated inside highly-detailed cosmological N-body simulations. They are useful to assemble a sample of DM halos, hosting galaxies made of BM, in order to follow the evolution of observables through cosmic times until $z = 0$. In this way, several properties of galaxies have been fully explored, like for instance stellar mass assembly inside DM halos (Moster et al. 2013), galaxy growth (De Lucia & Blaizot 2007) and population in cosmic epochs (Guo et al. 2011) and the SFRD(z) (Chiosi et al. 2017).

Aims of this study. The great success of the large scale simulations might lead us to conclude that no other alternatives are worth being pursued to investigate the formation and evolution of galaxies together with their large scale properties. However, major drawbacks of the massive numerical simulations are their complexity, high cost in terms of time and effort, and lack in flexibility and prompt response to varying key input physics. For these reasons we prefer to investigate the properties of the CMDs of cluster galaxies from a different perspective. The method we are going to propose is the same we have used to investigate the SFRD(z) in Chiosi et al. (2017). We start from suitable models of galaxies made of DM and BM that are able to catch the essence of NB-TSPH simulations of galaxy formation and evolution in the classical Λ -CDM cosmological model of the Universe, of which we exploit the number density of galaxies predicted by large scale N-Body simulations. With the aid of this, we predict the population of galaxies in clusters of typical size, and follow the photometric evolution of the model galaxies: we make use of the Monte-Carlo technique to simulate bursts of star formation in individual galaxies (age and intensity of the bursts are randomly chosen) and to simulate mergers among galaxies of different age, mass, chemical enrichment and stellar content. We derive the CMD and investigate how galaxies distribute in the three main groups. In particular we look at the physical status of the galaxies in the groups and under which conditions they pass from one group to

Table 1. The Color Magnitude Relation ($B - V$) = $(A \pm \Delta A) M_V + (B \pm \Delta B)$ of the Red Sequence for a selected sample of galaxy clusters from the WINGS Survey (Valentinuzzi et al. 2011).

Name	Number	A	$(\pm \Delta A)$	B	$(\pm \Delta B)$
A119	116	-0.042	0.007	+0.051	0.142
A168	118	-0.064	0.013	-0.458	0.266
A754	118	-0.042	0.006	-0.011	0.114
A970	117	-0.044	0.010	+0.046	0.198
A2399	116	-0.051	0.008	-0.198	0.169
A2457	114	-0.045	0.009	-0.022	0.181
A3158	122	-0.042	0.006	0.033	0.128
A3376	116	-0.045	0.009	-0.176	0.180
A3395	115	-0.037	0.007	0.044	0.133
A3809	119	-0.065	0.010	-0.516	0.217

another. We also examine and try to quantify the relative weight of the hierarchical aggregation compared to the intrinsic star formation history in galaxies of different mass. In particular we investigate the effect of galactic winds in shaping the color evolution of a galaxy.

The plan of the paper is as follows: in Section 2 we briefly present the CMDs based on the WINGS and OMEGA-WINGS surveys for the whole sample and also for a selected group of clusters of which we intend to interpret the CMDs with the aid of Monte-Carlo simulations based on both SSPs and realistic models of galaxies. In Section 3 we briefly present the main physical assumptions at the base of SSPs and model galaxies. In Section 4 we present the Monte-Carlo simulator of bursts of star formation in galaxies and mergers among galaxies, in which a generic galaxy is approximated to a SSP of suitable metallicity and age, and for these composite objects we derive the CMD. In Section 5 we extend the Monte-Carlo simulator of Section 4 by replacing the SSP with realistic models of galaxies. In particular we estimate the population of DM hosting BM galaxies with the aid of the HMF and HGF formalism (the definition of the latter will be given therein), derive the galaxy demography in clusters, generate the path of model galaxies in the CMD in presence of mergers, discuss the Red Sequence, Green Valley and Blue Cloud, and finally examine the star formation rate versus galaxy mass relationship. In Section 6 we draw some general conclusions and outline the plans for future studies. Finally, in Appendices A and B we present a few technical details in form of tables and figures that may be of general interest.

2. OBSERVATIONAL DATA AND CMR

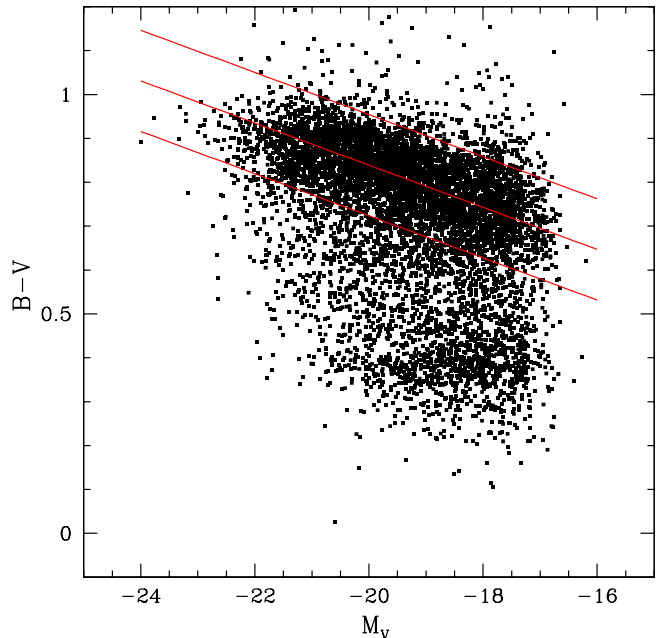


Figure 1. The total CMD for the 46 galaxy clusters by Cariddi et al. (2018). The red lines are the fiducial CMR derived from the entries for ten clusters of Table 1 with 1σ uncertainty on the zero-point.

In recent times, large optical and spectroscopic databases for the galaxy content of nearby clusters have become available thanks to the Wide-field Nearby Galaxy-cluster Survey (WINGS) of Fasano et al. (2006) and Varela et al. (2009) and companion OMEGA-WINGS extension of Gullieuszik et al. (2015) and Moretti et al. (2017) for a number of clusters in the redshift interval ($0.04 \leq z \leq 0.07$). All this material has been subsequently examined by Cariddi et al. (2018) with particular attention to the problems of the accurate determination of the stellar light and the stellar mass profiles of galaxy clusters. They measured and examined more than 7,000 galaxies in 46 clusters for which they provide the absolute V and B magnitudes, the morphological type according to the classification system RC3 by de Vaucouleurs et al. (1991), Corwin et al. (1994) and the extension made by Fasano et al. (2012), and the four different estimates of the star formation rates (SFR) by Fritz et al. (2007, 2011). The issue of membership of the galaxies to the clusters under consideration has been addressed and examined by Cava et al. (2009) to whom we refer for all details. In this study we have considered all the 46 clusters studied by Cariddi et al. (2018), however with particular attention to a subgroup of ten clusters for which more data were available. The list of ten clusters under examination is given in Table 1 which contains

the cluster identification (column 1), the total number of galaxies in each cluster (column 2), and the estimated color-magnitude relation (CMR) expressed by $(B - V) = (A \pm \Delta A) M_V + (B \pm \Delta B)$ (slope and zero point, columns 3 through 6): data related to the Red Sequence were derived by [Valentinuzzi et al. \(2011\)](#). From the CMR of ten clusters we derive the fiducial mean CMR: $(B - V) = -0.048M_V - (0.121 \pm 0.173)$ whose zero-point is estimated at 1σ uncertainty. This should roughly indicate the slope, width and location of the Red Sequence in the CMD. The $B - V$ color of each galaxy was derived here using the values of the B and V SExtractor `mag_auto` given by [Gullieuszik et al. \(2015\)](#) corrected for galactic extinction and K-correction. These are not aperture magnitudes but extrapolated values providing the total galaxy luminosity. The colors are therefore average values of the whole visible galactic components. The cumulative CMD for all galaxies in the full sample of clusters is shown in [Fig. 1](#) where the Red Sequence, the Green Valley, and the Blue Cloud are well evident. In this CMD we also plot the fiducial CMR for the ten best clusters (the red lines).

A few remarks are worth here: (i) The Red Sequence contains a few objects with unusual red color ($B - V \geq 1.1$). Their occurrence could be due to poor photometric data, wrong membership, and/or very high reddening. Since they are very few in number compared to the total, we simply drop them off the sample. The sample of ten reference clusters has been cured for the presence of these very red objects. (ii) Roughly speaking, the Green Valley is confined in the color range $0.6 < B - V < 0.8$, has nearly the same mean slope of the Red Sequence and is populated by fewer objects. The scarce population of the Green Valley suggests that galaxies in it are in rather quick evolutionary phases of their stellar content. (iii) Finally the Blue Cloud, customarily associated to galaxies with ongoing star formation (e.g. spirals and robust dwarfs), falls below the Green Valley and has a rich population. (iv) The sharp magnitude boundary at $M_V \simeq -17$ is merely due to observational detection limits of the survey and therefore is less of a problem. However, one should keep this in mind when comparing theoretical predictions to observational data at the low luminosity side of the CMD.

Now we separate galaxies of the full sample in two groups according to their morphological type: the first group named the *early-type galaxies* contains all the objects with RC3 type in $[-6, 0]$, whereas the second group named the *late-type galaxies* are objects with RC3 type in $(0, 11]$ ([Fasano et al. 2012](#), [Fasano et al.](#), in preparation). The two cumulative CMDs are separately shown in the left and right panels of [Fig. 2](#) together with the fiducial CMR as a reference (the solid black lines).

Looking at CMD for the two subgroups, contrary to what one naively could expect, the two distributions do largely overlap. Red spirals have been known for long time, they were called anemic spirals by [van den Bergh](#)

(1976), thought to be endemic to clusters of galaxies and recently rediscovered by the Galaxy Zoo collaboration ([Masters et al. 2010](#)). How can it be that a spiral galaxy has the same red color of an early-type? Misclassification? Very strong reddening? Most likely, in addition to classically referred factors like age and metallicity, both concurring to making a galaxy red, there is something else extinguishing star formation even in spirals and not only in early-type galaxies. The reverse side of the coin is that early-type galaxies deeply overlap the region that is typically populated by spirals and irregulars, making several early-type galaxies have same colors as late-type galaxies. To cast light on this issue, we derive the number distribution in color for the whole sample of galaxies. In order to better separate the two groups and better put in evidence the Green Valley, we apply a rotation of the CMD plane around a central point determined by visual inspection of the data (coordinates are $B - V = 0.70$ and $M_V = -20$) so that the projection on the $B - V$ axis is nearly parallel to the direction of the Green Valley, which in turn is nearly parallel to the Red Sequence. The choice of the center of rotation is not an severe issue and of course the rotation angle is very small. The results are shown in [Fig. 3](#). The comparison with the same diagram but without rotation (not shown here) soon clarifies that rotation does not affect our conclusion: the sample of early-type galaxies overlaps that of the late-type ones, and viceversa. It implies that the three loci in the CMD have boundaries not so strictly defined, with the Green Valley, in the middle of Red Sequence and Blue cloud, being populated by objects independently of their morphology.

It is worth recalling that while the red peak is quite robust, the height of the blue peak may be affected by a certain degree of incompleteness in the number of low luminosity galaxies. In any case, the key point we want to make here is that the two distributions greatly overlap, thus lending some support to the idea we would like to advance and explore in this study. In the environment of a cluster, spiral galaxies may lose their gas and soon after become red objects, whereas early-type galaxies may occasionally acquire some gas and by reviving their star formation activity becoming temporarily blue objects. Because of the gravitational confinement of the galaxies inside a cluster the above picture should be more probable than in the case of field galaxies, for which an evolutionary history in isolation should be more likely. Finally, we would like to note that the CMR for the ten best clusters is nearly indistinguishable from the one displayed in [Fig. 1](#). In the following when comparing theory with observations we will make use of the former for the sake of clarity.

As a final remark, we would like to remind the reader that in this study we consider each galaxy cluster as a whole leaving aside the possible radial dependence of the galaxy content (i.e. morphological type, galaxy mass, mean star formation rate of each galaxy, etc...) and the

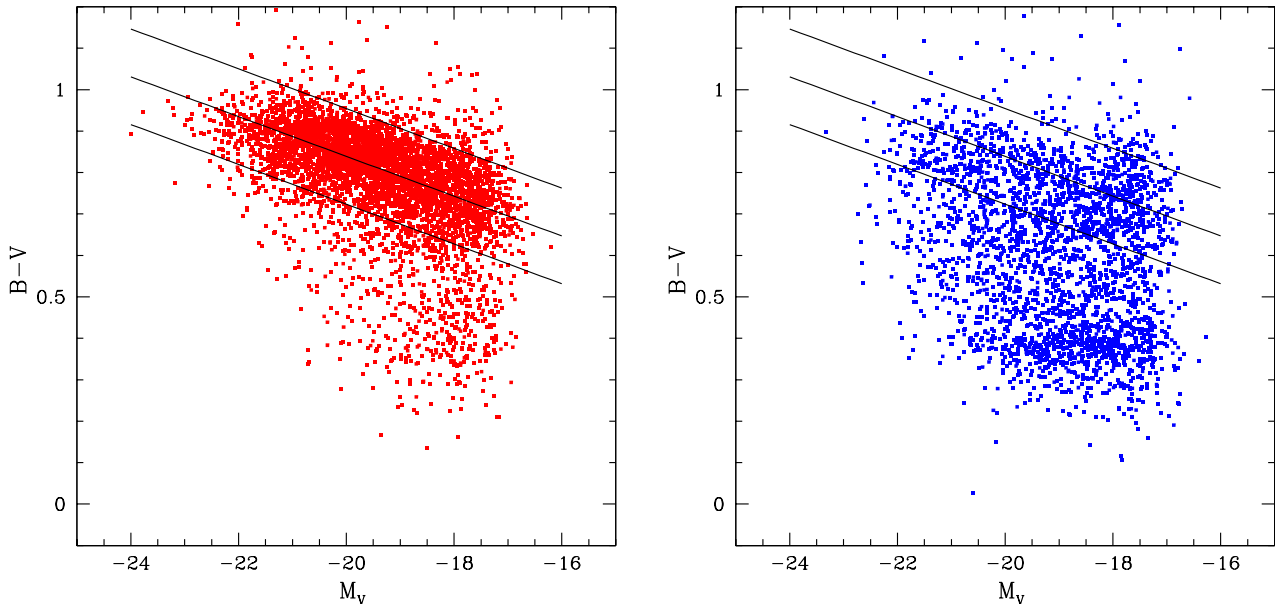


Figure 2. Left Panel: The CMD for early-type galaxies (from cD through S0/a) of all the 46 clusters of Cariddi et al. (2018). The black lines are the fiducial CMR of the ten clusters listed in Table 1 with 1σ uncertainty on the zero-point. Right Panel: the same as in the left panel but for late-type galaxies from Sa through cI.

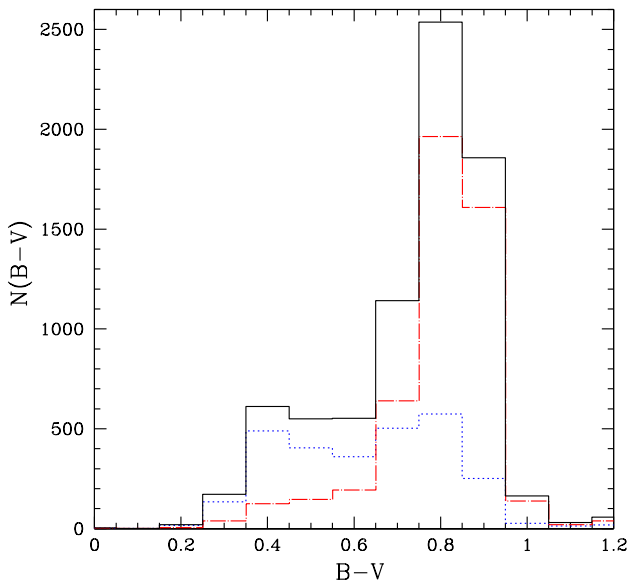


Figure 3. Histograms of the number vs $B - V$ color for all the galaxies of the full sample. The dashed red line is for early-type galaxies CM (from cD through S0/a); the dotted blue line is for late-type galaxies (from Sa through cI); finally the solid black line is for the two groups of galaxies together. Rotation of the original CMD has been applied, so that the projection onto the $B - V$ axis is parallel to the direction of the the mean CMR.

presence of diffuse intra-cluster medium that could affect the evolution of a generic galaxy via the possible effects of gas stripping and harassment. Each CMD is built by plotting the integrated colors and magnitudes of each galaxy without considering the geometrical structure of the cluster itself.

3. BARYONIC MATTER IN DARK MATTER HALOS: GALAXY MODELS

In this section we briefly introduce the models we have used to describe galaxies in terms of chemical evolution and photometric. For the sake of our investigation, we make use of both single stellar populations (SSPs), with suitable chemical composition (the “metallicity” Z) and age, and of simple model galaxies based on the one-zone description, which is proven to successfully describe the star formation and metal enrichment histories and the photometric properties of galaxies in cosmological contexts (in addition to following Subsections and works therein referred to, we refer the reader to Chiosi 1980; Tantalo et al. 1996; Portinari et al. 1998; Chiosi et al. 2017, for full descriptions of the models).

3.1. Single Stellar Populations: spectra, magnitudes and colors

The classical tool for this kind of studies is the evolutionary population synthesis (EPS) introduced long ago by Tinsley (1968, 1980) and ever since developed to a high degree of sophistication by many authors (Bressan et al. 1994; Tantalo et al. 2010; Conroy 2013; Conroy et al. 2014; Pasha et al. 2018; Dahmer-Hahn et al. 2018, and references).

In the following we adopt the method developed by [Bressan et al. \(1994\)](#). The monochromatic flux generated by the stellar content of a galaxy of age T_G is defined as:

$$F_\lambda(T) = \int_0^T \Psi[t, Z(t)] sp_\lambda[\tau', Z(\tau')] dt \quad (1)$$

where $\Psi[t, Z(t)]$ is the SFR at the age t and metallicity $Z(t)$ (chemical content in general), $sp_\lambda[\tau', Z(\tau')]$ the integrated monochromatic flux of a single stellar population (SSP), a coeval chemically homogeneous assembly of stars, with given age $\tau' \equiv T_G - t$ and $Z(\tau')$. The flux of a SSP is in turn given by

$$sp_\lambda[\tau', Z(\tau')] = \int_{M_l}^{M_u} \phi(M) f_\lambda[M, \tau', Z(\tau')] dM \quad (2)$$

where $\phi(M)$ is the stellar initial mass function (IMF) and $f_\lambda[M, \tau', Z(\tau')]$ is the monochromatic flux of a star of mass M inside the SSP. M_l and M_u denote the mass range within which stars are generated by each event of star formation. The metallicity dependency of SFR $\Psi(t, Z)$ is customarily neglected and so it is for the time and metallicity of the IMF. Sources of stellar tracks, isochrones, spectra, and SSPs in different photometric systems are from [Bertelli et al. \(2008, 2009\)](#); [Tantalo \(2005\)](#).

In this paper we adopt the IMF of [Salpeter \(1955\)](#), which is $\Phi(M) \propto M^{-2.35}$. It is normalized by choosing the fraction ζ of stars more massive M_n , i.e. the mass interval most contributing to chemical enrichment over the whole Hubble time:

$$\zeta = \frac{\int_{M_n}^{M_u} \phi(M) M dM}{\int_{M_l}^{M_u} \phi(M) M dM} \quad (3)$$

where M_n and M_u are fixed to $M_n \simeq 1 M_\odot$ and $M_u = 100 M_\odot$, and M_l follows from the normalization.

The database of SSPs in use has been computed by [Tantalo \(2005\)](#) adopting the library of stellar spectra assembled by [Girardi et al. \(2002\)](#), for ages between 10^7 yr and 13×10^9 yr, metallicities from $Z = 0.0001$ to 0.1 , and for seven different prescriptions of the IMF. Fluxes, and hence magnitudes, are calculated for the total mass of a SSP:

$$\int_{M_l}^{M_u} M \Phi(M) dM = M_{SSP}. \quad (4)$$

The total mass of the SSP depends on the IMF and the values of M_l and M_u .

The SEDs of SSPs mirror the SED of all component stars along the isochrones and how stars of different mass populate an isochrone. Therefore, the magnitudes and colors of SSPs depend on a complicated game among all those players and consequently differences among the

many sources of SSPs in literature are expected (see [Tantalo 2005](#)). In this study we adopt the wide tabulations of SSPs magnitudes as function of age and chemical composition and IMFs calculated by [Tantalo \(2005\)](#) for a large grid of photometric systems going from: classical Johnson, Bessell-Brett, Hubble Space Telescope (NICMOS, WFPC2, ACS), to the Sloan Digital Sky Survey (SDSS), 2MASS, and others. All details about the photometric pass-bands and definition of the magnitudes systems can be found in [Tantalo \(2005\)](#); [Tantalo et al. \(2010\)](#).

It is worth recalling here that in recent times evolutionary tracks with chemical composition including the enhancement of α -elements (like Carbon, Oxygen, Titanium etc.) have been calculated (see e.g. [Salasnich et al. 2000](#); [Fu et al. 2018](#), and references). Therefore, the parameter $[\alpha/Fe]$ should be added to those characterizing the chemical pattern of elements, and SSPs including its effect should be considered. However, as the tabulations of SSPs with α -enhancement in the Padua database to our disposal are not large enough for our purposes, we do not include this effect in our analysis. In any case, they will induce second order effects on the dominant ones given by the metal content Z .

Finally, we would like to comment that as far the integrated spectro-photometric properties of complex stellar populations (stellar clusters and galaxies) are concerned magnitudes and colors do not much depend on the underlying IMF, whereas the mass-to-light ratios are sensitive to this parameter. This can be easily understood by means of the following simple arguments. Excluding the more intrigued case of very young SSPs in which massive stars are present, at increasing age very soon SSP reaches the regime in which most of the light come from evolved stars in the post main sequences stages (red giants, clump and/or horizontal branch stars, asymptotic giant branch stars), the rest from main sequence objects at or just below the turn off. The remaining main sequence stars play a minor role. On the other hand the post main sequence stars of a SSP span a rather narrow range of masses. Therefore, to induce a significant effect on the photometric properties (magnitudes and colors), the slope of the IMF should vary a lot over the post main sequence mass interval. This is not the case for all IMF in literature. Therefore, the use of the Salpeter IMF is fully justified and adequate to our purposes. However, for the sake of clarity and comparison, in [Appendix A](#) we provide a summary of the SSP magnitudes and colors limited to the solar composition (metallicity $Z = 0.019$), the Johnson-Bessell-Brett system, and three different very popular IMFs ([Salpeter 1955](#); [Chabrier et al. 2014](#); [Kroupa 2008](#), and references). All other details can be found in [Tantalo \(2005\)](#). The use of the Salpeter IMF is also supported by the study of field and cluster ellipticals at intermediate redshifts by [Schade et al. \(1996\)](#).

3.2. Simple Galaxy Models

In this study, we adapt the multi-shell spherical models of galaxies developed by [Tantalo et al. \(1998\)](#) to the one-zone description, which is fully adequate to our purposes. These galaxy models include many important physical phenomena, for instance gas heating by supernova explosions (both type Ia and type II), stellar winds, gas cooling by radiative emission, galactic winds, and the presence of DM in shaping the gravitational potential. In brief, the galaxy of total mass M_G is made by the BM component with mass M_{BM} and DM component with mass M_{DM} , according to

$$M_G(t) = M_{BM}(t) + M_{DM} \quad (5)$$

The DM mass is supposed to be present from the very beginning with a suitable spherical distribution so that its contribution to the gravitational potential is fixed. The BM mass is supposed to be originally in form of gas, to flow in at suitable rate, to build up its own gravitational potential and, when physical conditions allow it, to transform into stars. This kind of model, originally developed by [Chiosi \(1980\)](#), is named the infall model, the essence of which resides in the gas accretion into the central region of the proto-galaxy at a suitable rate (driven by the timescale τ) and in the gas consumption by a Schmidt-like law of star formation. The gas accretion and consumption coupled together give rise to a time dependence of the SFR closely resembling the one resulting from the N-body simulations (e.g. [Chiosi & Carraro 2002](#); [Merlin & Chiosi 2006, 2007](#); [Merlin et al. 2012](#)). At this point we warn the reader that, throughout this work, whenever we use the expressions formation time (redshift) or age of a galaxy we refer to the beginning of baryonic history; the viceversa is also true.

At any time t the baryonic mass M_{BM} is given by the sum

$$M_{BM}(t) = M_g(t) + M_*(t) \quad (6)$$

where $M_g(t)$ is the gaseous mass and $M_*(t)$ the star mass. At the beginning, both the gas and the star mass in the proto-galaxy are zero $M_g(t=0) = M_*(t=0) = 0$. The rate of BM (and gas in turn) mass accretion is driven by the accretion timescale τ according to

$$\frac{dM_{BM}(t)}{dt} = M_{BM,\tau} \exp(-t/\tau) \quad (7)$$

where τ is the accretion timescale and $M_{BM,\tau}$ a constant with the dimensions of [Mass/Time] to be determined by imposing that at the galaxy age T_G the total baryonic mass of the galaxy $M_{BM}(T_G)$ is reached:

$$M_{BM,\tau} = \frac{M_{BM}(T_G)}{\tau[1 - \exp(-T_G/\tau)]}. \quad (8)$$

Therefore, integrating the accretion law the time dependence of $M_{BM}(t)$ is

$$M_{BM}(t) = \frac{M_{BM}(T_G)}{[1 - \exp(-T_G/\tau)]} [1 - \exp(-t/\tau)]. \quad (9)$$

The timescale τ parameterizes the timescale over which the present-day mass $M_{BM}(T_G)$ is reached, because it is related to the average rate of gas cooling and it is expected to depend on the mass of the system. In this scheme the total mass of a galaxy at the present time is $M_G = M_{DM} + M_{BM}(T_G)$.

While in the earliest stages of a galaxy M_{BM} can be considered equal to M_g , soon after the gas cools down and star formation begins. We model this throughout the whole life of the galaxy with a Schmidt-like law of star formation ([Schmidt 1959](#)):

$$\Psi(t) \equiv \frac{dM_*}{dt} = \nu M_g(t)^k \quad (10)$$

where k regulates the dependency of SFR on gas content (classically it can be linear or quadratic: we fix it as $k = 1$) and ν is the efficiency parameter of the star formation process.

In the infall model, because of interplay between gas accretion and consumption, the SFR starts low, reaches a peak after a time approximately equal to τ and then slowly declines. The functional form that could mimic this behavior, with systematic variation with mass, is the delayed exponentially declining law:

$$\Psi(t) \propto \frac{t}{\tau} \exp\left(-\frac{t}{\tau}\right). \quad (11)$$

The Schmidt law in eqn. (10) is therefore the link between gas accretion by infall and gas consumption by star formation.

As a whole, this kind of approach stands on a number of observational and theoretical arguments among which we recall (i) the parameters ν and τ can be related to morphology ([Buzzoni 2002](#)) and to the presence of on-going star formation activity inside observed galaxies ([Cassarà et al. 2016](#)); (ii) the aforementioned quantities can be easily tuned in order to fit observational data, and also complex phenomena that would affect the rate of gas cooling, such as active galactic nuclei (AGN), can be empirically taken into account without going into detail (see e.g. [Chiosi et al. 2017](#)).

3.2.1. Energy feedback, gas heating-cooling, galactic winds

Long ago [Larson \(1974\)](#) postulated that the present-day CMR of elliptical galaxies (see also [Terlevich et al. 2001](#), and references) could be the result of galactic winds powered by supernova explosions: a long series of chemo-spectro-photometric models of elliptical galaxies stemmed from this idea ([Tantalo et al. 1996](#);

Table 2. The key parameters of the model galaxies: mass, ν and τ . Masses are in solar units.

Type	log M	7	8	9	10	11	12	13
ET _{<i>ms</i>}	τ	6	5	4	3	2	2	1
ET _{<i>ms</i>}	ν	10	10	10	10	10	10	10
ET _{<i>gw</i>}	τ	6	5	4	3	2	2	1
ET _{<i>gw</i>}	ν	10	10	10	10	10	10	10
LT _{<i>ms</i>}	τ	10	8	6	4	3	2	1
LT _{<i>ms</i>}	ν	1	1	1	1	1	1	1

Gibson & Matteucci 1997; Tantalò et al. 1998, and references therein). In brief, gas is let escape from the galaxy and star formation is supposed to halt when the total thermal energy of the gas equates its gravitational binding energy.

The thermal energy of the gas is mainly due to four contributions, namely Type Ia and II supernovae, stellar winds from massive stars, and AGNs (these latter however are not included here; see above):

$$E_{th}(t) = \sum_J E_{th}(t)_J \quad (12)$$

where J indicates the various sources of heating (see Tantalò et al. 1998, for all details). Suffice to recall here that the injected energies incorporate the cooling laws of supernova remnants and stellar winds by radiative cooling processes. The condition for the onset of the wind is

$$E_{th}(t) \geq |\Omega_g(t)| \quad (13)$$

where Ω_g is the gravitational potential energy of the gas. To determine this latter one needs to know the total gravitational potential of DM and BM together Ω_{DM+BM} . We strictly follow the assumptions and formalism of Tantalò et al. (1998) to whom the reader should refer for all details. We only mention here that Ω_{DM+BM} is a function of the ratios M_{BM}/M_{DM} and R_{BM}/R_{DM} , with obvious meaning of the symbols. In conditions of mechanical equilibrium and with the current estimates of M_{DM} and M_{BM} of the Λ -CDM cosmogony (see below), both ratios are equal to 0.16. With these values, the DM gravitational potential does not exceed 0.3 of that by the sole BM.

3.2.2. SFR and galactic winds

In the wind model of Larson (1974), when condition of eqn. (13) is verified, all the gas freely escapes from the galaxy so that further star formation does no longer occur. The evolution of the remnant galaxy is a passive one and all the gas shed by stars formed in the previous epochs, either in form of stellar wind or supernova

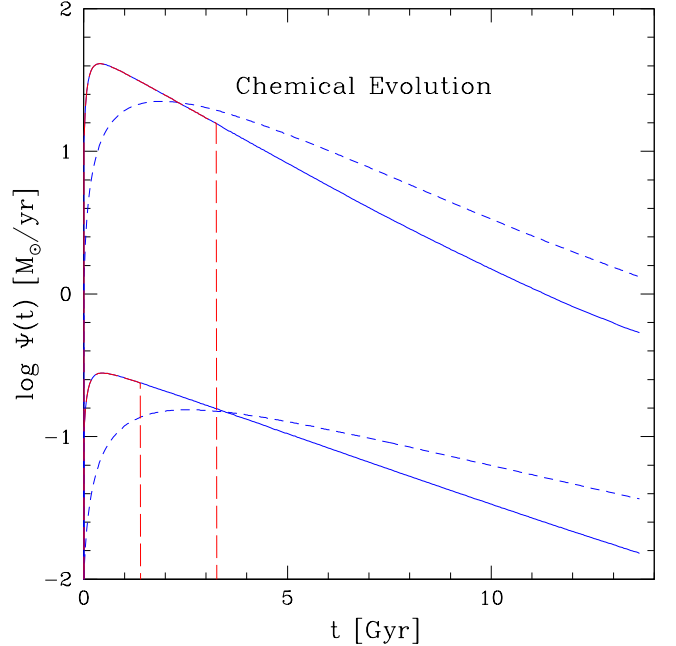


Figure 4. The SFR (on logarithmic scale) versus age of model galaxies. The blue solid lines indicate models labeled ET_{*ms*}, the blue short-dashed lines those labeled LT_{*ms*}, and the long-dashed lines those named ET_{*gw*}. Two model galaxies are displayed with different mass, i.e. 10^9 (bottom) and $10^{11} M_{\odot}$ (top).

explosion, does no longer generate new stars. In addition to this, owing to the different gravitational potential well of massive galaxies with respect to the low-mass ones, the time at which the threshold energy for galactic winds is reached occurs earlier in low-mass galaxies than in the massive ones. In contrast, more sophisticated treatments of winds with the aid of NB-TSPH models of galaxy formation and evolution (Chiosi & Carraro 2002; Merlin & Chiosi 2006, 2007; Merlin et al. 2012) have shown that galactic winds are not instantaneous but take place on long timescales. Gas heated up by supernova explosions and stellar winds and cooled down by radiative processes not only gradually reaches the escape velocity but also affects the efficiency of star formation because the hot gas is continuously subtracted. To take this into account in our simple models, we proceed as follows.

First of all, feeling that the cooling algorithm we are using is not as good as the one currently adopted in NB-TSPH models, we introduce an efficiency parameter η_{th} ranging from 0 (no energy feedback) to 1 (full energy feedback) and accordingly change the (13) to the new one

$$\eta_{th} \times E_{th}(t) \geq |\Omega_g(t)| \quad (14)$$

Second, we change the star formation law of eqn. (10) redefining the parameter ν as an effective efficiency given by

$$\nu_{eff} = \nu \times \frac{|\eta_{th} \times E_{th} - |\Omega_g||}{\eta_{th} \times E_{th} + \Omega_g} \quad (15)$$

where ν is the usual efficiency. By decreasing the efficiency of star formation at increasing E_{th} we intend to mimic the fact that hot gas is likely less prone to generate stars by gravitational collapse. As a consequence, the threshold stage for the onset of galactic winds may occur much later in time or even avoided at all. Less gas is turned into stars as if part of the gas is continuously escaping from the galaxy. For the aims of this study, we tune the parameter η_{th} in such a way that the SFR is reduced but never extinguished during the whole galaxy lifetime. We refer to these as models with “modulated star formation” (ms). In parallel we also calculate models with the standard prescription for the galactic wind. These are referred as models with “galactic wind” (gw).

Finally we calculate models with two different combinations of the parameters τ and ν that are chosen in such a way that (i) the peak of star formation occurs early on in the galaxy life and then significantly declines; these are named “Early-Type (ET) models with modulated star formation” because they are meant to simulate early-type galaxies; (ii) the peak of star formation occurs at early times but star formation continues at rather high levels of efficiency till the present epoch; these models are meant to simulate either spiral or dwarf galaxies and are indicated as Late-Type (LT). In total, we have the following cases: ET_{ms}, ET_{gw}, and LT_{ms}. The adopted values for the parameters τ and ν are summarized in Table 2. The time dependence for the above three cases is shown in Fig. 4 for two values of the galaxy mass. We highlight that (i) ET_{ms} and ET_{gw} models are identical until gas escapes completely at the onset of winds for the ET_{gw} ones (ii) SFR turns off with age increasing with the mass of the system.

3.2.3. Galaxy Photometry

The EPS technique and the concept of SSPs allow us to derive the SED of a galaxy under any history of star formation and chemical enrichment. Knowing the SED and the photometric system in use, magnitudes and colors as function of the age and chemical parameters are straightforward; the procedure is the same as in Bressan et al. (1994). Here we limit ourselves to quickly address the issue of the dust. Magnitudes and colors of both SSPs and galaxies are affected by the presence of dust. In the case of SSPs, dust is always present in the envelopes of O-type and AGB stars (i.e. at young and oldish ages), so that attenuation of radiation occurs in the stellar nearby. In addition, additional reddening affects radiation before it escapes completely from a galaxy due to interstellar dust

(see Piovan et al. 2006b,a, 2011c,b,a; Cassarà et al. 2013; Salaris et al. 2014; Cassarà et al. 2015, for exhaustive discussions and technical details). In this paper, the self-attenuation of the spectrum of young and oldish SSPs is already included in the dataset in use, while for galaxies we proceed as Bressan et al. (1994) and adopt the simple method of Guiderdoni & Rocca-Volmerange (1987). In brief, they introduce the effective optical thickness of the gaseous component at the wavelength λ :

$$\tau_\lambda = 3.25(1 - \omega_\lambda)^{0.5}(A_\lambda/A_V)_\odot [Z(t)/Z_\odot]^s G(t) \quad (16)$$

where ω_λ is the albedo of dust grains, for which we take the mean value 0.4 (Draine & Lee 1984), A_λ/A_V the extinction law (here we adopt the relation by Cardelli et al. 1989), $s = 1.3 - 1.4$ for $\lambda \leq 2000 \text{ \AA}$ and $s = 1.6$ for $\lambda \geq 2000 \text{ \AA}$, and $G(t)$ the gas fraction. The optical depth τ_λ is used to derive the transmission function for an angle of inclination i . The transmission function is defined as

$$\frac{1 - \exp(-\tau_\lambda \sec i)}{\tau_\lambda \sec i} \quad (17)$$

by which we multiply the monochromatic flux of the rest-frame SED of the model galaxies. We adopt here the constant inclination angle $i = 0^\circ$.

3.3. Passing from rest-frame to cosmological evolution of SSPs and galaxies

The SSPs and galaxies are let evolve from the redshift of formation z_f to the present $z = 0$, i.e. from the rest-frame age $T = 0$ Gyr to the maximum age T_G Gyr where $T_G = T_U(z = 0) - T_U(z = z_f)$ with $T_U(z)$ being the age of the Universe for the adopted cosmological model. If for any reason, we need to change the redshift of galaxy formation from z_f to z_f^* (keeping unchanged all other input parameters) the same models can be used provided their rest-frame age is simply limited to the interval from $T = 0$ at z_f^* to $T_G^* = T_{G,(z_f)} - T_U(z_f^*)$, where $T_U(z_f^*)$ is the age of the universe at $z = z_f^*$. The cosmological model of the Universe is the Λ CDM concordance cosmology, with the parameters inferred from WMAP-7 data (Komatsu et al. 2011): $H_0 = 70.4 \text{ km s}^{-1} \text{ Mpc}^{-1}$, $\Omega_\Lambda = 0.73$, $\Omega_m = 0.27$, $\Omega_b = 0.05$, $\sigma_8 = 0.81$, and $n = 0.97$.

4. PLAYING WITH SSPs: BURSTS AND MERGERS

In this section we present a preliminary analysis of CMDs of cluster galaxies using only SSPs of different ages and metallicities: masses are set equal to those of typical galaxies in the mass interval 10^7 to $10^{13} M_\odot$. We call this type of galaxy model *SSP-galaxies*. To this aim we set up Monte-Carlo simulations of bursts of star formation in already existing seed objects of mass, age and

Table 3. Empirical mass-metallicity relation for SSP-galaxies. Logarithmic masses are in solar units.

$\log M$	7 - 8	8 - 9	9 - 10	10 - 11	11 - 12	12 - 13
Z_{min}	0.0004	0.001	0.004	0.008	0.019	0.040
Z_{max}	0.0010	0.004	0.008	0.019	0.040	0.070

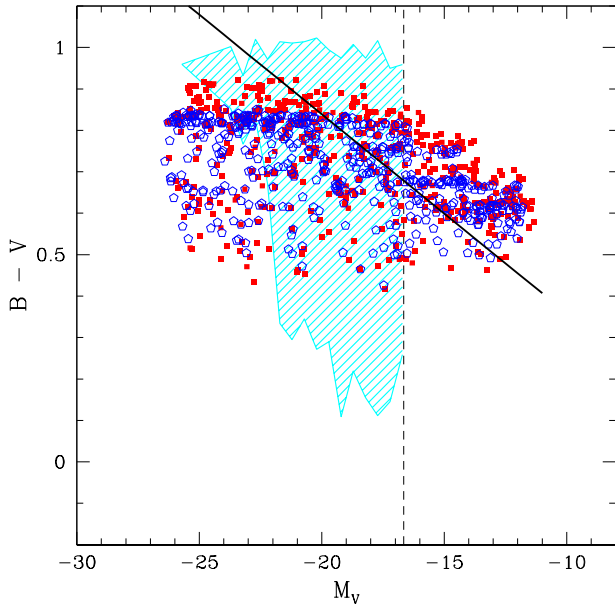


Figure 5. Simulation of 500 SSP-galaxies with $T_{G,max} = 13$ Gyr (red solid squares) and $T_{G,max} = 6$ Gyr (blue open pentagons), which underwent a single burst with $T_{B,max} = 5$ Gyr and mass fraction of 5%, observed at $z = 0$. WINGS data related to the ten best clusters (cyan shaded area) are shown for comparison; the dashed vertical line represents the faintest object in the WINGS dataset. The black solid line is the fiducial mean CMD already discussed in Sect. 2. It is worth noting the discrepancy between the fiducial CMD and the distribution of the red galaxies on the CMD. First for galaxies brighter than $M_V \simeq -20$ the fiducial CMD is steeper than the models, second for fainter galaxies the slope is nearly the same but the models are redder than the observed galaxies. On one hand the zero point of the fiducial CMD is uncertain, on the other hand the burst models may not be fully suited to represent real galaxies.

metallicity, and of mergers among galaxies of different age, metallicity and mass. We compare the results of both simulations are compared both with observational data related to the ten best WINGS clusters described in Section 2.

4.1. Bursts and mergers

As a first step, we approximate the complex mix of stellar populations inside a galaxy of mass M_G with a SSP of suitable age T_G , metallicity Z_G and the same

mass. T_G , Z_G are the age and metallicity reached at the peak of star formation, which according to current galaxy models occur shortly after the formation of the galaxy itself (Chiosi et al. 2017) so that $T_G(z_G)$ roughly corresponds to the formation time (redshift). With T_U the present age of the Universe for the adopted cosmological scenario, then $T_{G,z} = T_U - T_G$ is the age (redshift) of the Universe when the galaxy was born.

In the following, we will explore two paradigmatic cases: (i) An already in place galaxy via the initial major episode of star formation, which later undergoes an additional episode of star formation of minor intensity (thereafter referred as *burst* case). With simulations of this kind, we explore the consequences of adding young stellar components to already evolved stellar assemblies, in other words we can estimate the effect of a rejuvenation event on an otherwise passively evolving stellar system. This is the analog of simulating either completely wet mergers or a minor stellar activity for any internal reason (eg. re-use of the gas shed by RGB and AGB stars). (ii) The other interesting case to consider is the case of a *merger* of two galaxies of different mass, age, and metallicity. This would simply tell us how the photometric properties of each of the two subsystems added together would give rise to a new photometric appearance of the composed system even in absence of companion star formation. This is the analog of a random combination of wet and dry mergers.

Bursts. The age T_G of the initial star forming episode is supposed to fall in the age range $T_{G,max} > T_G > T_{G,min}$. Subsequently, a burst of star formation engaging a certain percentage of the mass (typically up to about 10%) is supposed to occur at any age T_B comprised between $T_{B,max} = T_{G,min}$ and the present time (more precisely $T_{B,min} = 0.1$ Gyr, the minimum age in the SSP grids).

The rest of the procedure is quite simple: first, we take the fluxes from SSPs of different metallicities, normalize them to unit of mass (with the Salpeter IMF and $M_l = 0.1 M_\odot$ and $M_u = 100 M_\odot$, $M_{SSP} = 5.826 M_\odot$), and then multiply them by the mass of the galaxy. Next, we randomize ages and masses of the seed SSP-galaxies together with the age and mass percentages of the burst episode. To this aim, it is more convenient to express the age and masses in terms of their logarithms, in order to avoid non-uniform distribution in the randomly chosen values. The ages (written with lower case symbols to

remind the reader that they are expressed as logarithms) of the seed galaxies are given by

$$t_G = t_{G,max} - r(t_{G,max} - t_{G,min}) \quad (18)$$

and those of the bursts by

$$t_B = t_{B,max} - r(t_{B,max} - t_{B,min}); \quad (19)$$

$r \in (0, 1)$ is a random, always different number. Similar procedure is made for the mass of the seed SSP-galaxy, which spans the range 10^7 to $10^{13} M_\odot$, and the mass percentage p_B of the burst mass with respect to the mass of the host galaxy. The percentage p_B goes from 0 to 0.05. Therefore, the relative contribution of the two components to the total flux (magnitudes in any pass-band) is given by

$$f = (1 - p_B) f_G + p_B f_B$$

with obvious meaning of the symbols. Finally, since the SSP fluxes (magnitudes and colors) depend on both age and metallicity and we know that this latter in turn increases with the galaxy mass, we have taken this into account by adopting an empirical mass-metallicity relation that is based on chemical models of galaxies and observational data and is presented here in Table 3. Shortly speaking, metallicity is for simplicity binned in terms of logarithmic mass.

Mergers. The mass, metallicity and age of each galaxy are derived using the same procedure as above, the only difference being that the permitted age interval extends now over nearly the whole Hubble time i.e. $T_{G,max} - T_{G,min} \simeq T_{G,max}$. Denoting with $T_{G,j}$ the age of the j -th component of the merger (a single event for simplicity) and using the logarithmic notation, the ages $t_{G,j}$ are

$$t_{G,j} = t_{G,max,j} - r t_{G,max,j} \quad (20)$$

where r is the random number. When two galaxies merge together, in the resulting bigger object there are stars from both initial components. At each time, their contribution to the total flux is first suitably shifted by the age difference between the two components to set up a common clock and then weighed by the mass of each component.

To keep our argumentations simple, we will treat mergers as single pairs of galaxies. In addition to this, we do not consider the case of multiple mergers first for the sake of simplicity and second because they seem to become inefficient as the clusters reach virialization (Merritt 1988; Richstone 1990). In the following we present some simulations of mergers and their effect on the CMD.

Remarks. In the simulations below, we will use only SSP with solar partition of α -elements, i.e. $[\alpha/Fe] = 0$. For each burst, metallicity is for simplicity chosen to be equal to that of the seed galaxies: this means

that, at variance with mergers, metallicities will not mix together.

4.1.1. Results

Bursts. In Fig. 5 we give a first insight on the impact by young stars polluting the light emitted by evolved stellar populations: we simulate single bursts, with $T_{B,max} = 5$ Gyr and $T_{B,min} = 0.1$ Gyr and a mass fraction of 5%, inside already existing SSP-galaxies with formation interval comprised between (i) $T_{G,max} = 13$ Gyr and $T_{G,min} = 5$ Gyr (red solid squares) and (ii) $T_{G,max} = 6$ Gyr and $T_{G,min} = 5$ Gyr (blue open pentagons). It is worth noting first the broad interval for the formation of bulk galaxy in the case (i), and the extreme, largely unrealistic, recent age for the bulk activity of case (ii).

After mass and metallicity are fixed, a complex interplay between ages of galaxy and burst is at work. As it will be better shown by means of detailed chemophotometric models of galaxies with infall of gas, the generation of new bright stars strongly enhances the emission in the blue side of a galaxy spectrum. Indeed looking at the two different sets of simulations with SSP-galaxies, it can be already seen that the main effect is a shift towards bluer colors and brighter luminosities in the V band. Even if we are treating single burst events, Green Valley and Red Sequence are already in place, although the latter appearing by-eye less steep than the one indicated by the WINGS data (black solid line) in the range of high mass SSP-galaxies, whereas for lower mass the agreement with observational data is nearly good. Changing $T_{G,max}$ while keeping fixed $T_{B,max}$ leads to a broadening of the Red Sequence, with the color $B - V$ becoming redder at increasing ages of the seed galaxies. Several comments are necessary here. First, we note a large discrepancy between the fiducial CMR and the distribution of the red galaxies on the CMD. For galaxies brighter than $M_V \simeq -20$ the fiducial CMR is steeper than the models, whereas for fainter galaxies the slope is nearly the same but the models are redder than the observations. Even if the zero point of the fiducial CMR is uncertain, this may suggest that the burst models are not fully suited to represent real galaxies. Second, very few SSP-galaxies fall into the region of the Blue Cloud. This means that much larger amounts of young stellar populations should be present inside galaxies of intermediate mass to get the lowest values of $B - V$. We could repeat the experiment by applying more massive bursts, however we prefer not to go further because another point of concern is also evident. Third, a large number of SSP-galaxies fall into the region of high luminosities ($M_V \lesssim -23$) and blue colors ($B - V \lesssim 0.8$) contrary to what shown by the observational data. This latter aspect will be fully clarified while dealing with mergers. Finally the models extend to magnitudes fainter than the observational ones, but

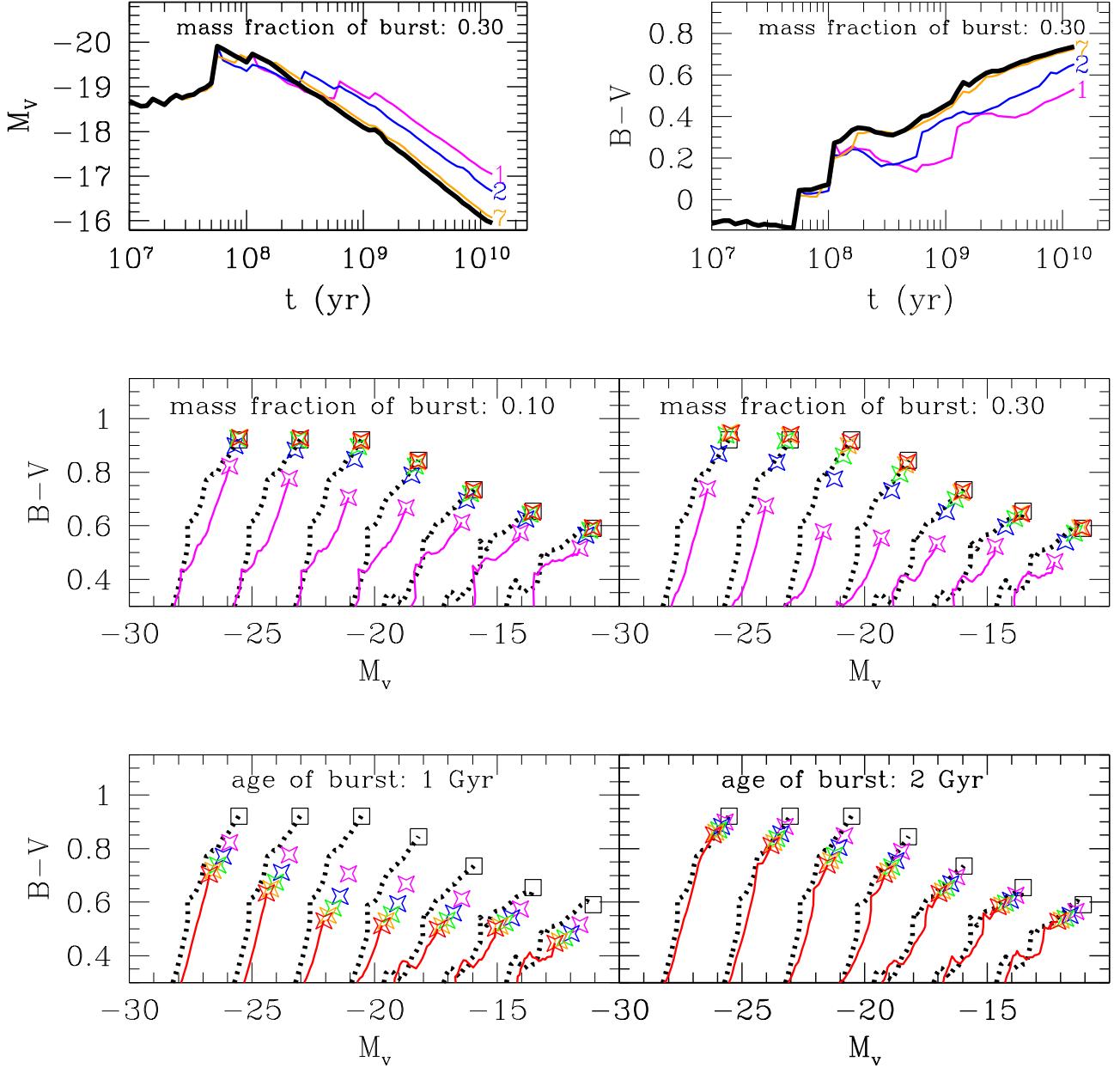


Figure 6. Results of dissection of single bursts inside 13 Gyr-old SSP-galaxies. **Upper Panels:** evolution with time of M_V (right) and $B - V$ (left) for the SSP-galaxy with $\log M = 9$ ($Z = 0.004$) perturbed by a single burst with mass fraction of 30%; solid thin curves are, in terms of increasing age, magenta (1 Gyr), blue (2 Gyr) and orange (7 Gyr); the thick black line is the unperturbed case shown for comparison. **Middle Panels:** CMDs of SSP-galaxies with fixed mass fraction of burst for a set of different ages of bursts, observed at $z = 0$: open stars indicate the final values reached by each perturbed case; colors are, in terms of increasing age, magenta (1 Gyr), blue (2 Gyr), green (4 Gyr), orange (7 Gyr) and red (8.5 Gyr); the path followed by the most extreme case is shown with a thin magenta line; the unperturbed case is shown as well (dotted black line ending with an open square). **Lower Panels:** same as Middle Panels, but with fixed age of burst for a set of different per cent masses of bursts: colors are, in terms of increasing percentage, magenta (10%), blue (20%), green (30%), orange (40%) and red (50%); the path followed by the most extreme case is shown with a thin red line; again the unperturbed case is shown as well (dotted black line ending with an open square)

this is less of a problem because of the photometric incompleteness of the data.

To cast light on the results presented in Fig. 5 we set $r = 0$ in eqns. (18) and (19) and fix the burst age at some pre-selected values. The results of these experiments are shown in Fig. 6. In the upper panels, we display the photometric evolution of a reference SSP-galaxy with mass $\log M = 9$, metal content $Z = 0.004$ basing on the empirical for the mass-metallicity relation, and age 13 Gyr. We show the unperturbed case (thick black line) together with three cases of single bursts with the same fractionary mass (30%) and different ages, namely 1, 2, and 7 Gyr, represented by the magenta, blue and orange lines respectively. The situation is immediately clear: we see that the younger the burst, the greater is the difference in terms both of magnitudes and colors. Moreover, the 7 Gyr line stands always very close to the unperturbed case despite the high intensity of the burst: this tells us that an old burst does not alter significantly the photometric appearance of an old galaxy. At decreasing age of the burst, the effect of this becomes larger and larger. Interestingly, a 2 Gyr-old burst leads to an intermediate state between 1 Gyr and 7 Gyr, confirming that the bulk of luminosity comes from rapidly evolving, very bright stars. As a final remark, we warn the reader that slight differences occurring at ages younger than 10^8 yr may be numerical and not strictly physical.

To better understand the consequences of bursts on the magnitudes and colors of a hosting galaxy, in the middle and lower panels of Fig. 6 we show a set of bursts applied to SSP-galaxies of different mass (for all the values listed in Table 3) at varying the burst intensity and age. For each case, the metallicity of the SSP-galaxy and the companion burst vary according to the mass-metallicity relation of Table 3. For each case, the dotted line is the unperturbed SSP-galaxy and the open square shows the present-day stage. The solid lines are the most extreme case for the burst either in age (middle panels) or intensity (bottom panels), whereas the open stars are the corresponding end-stages. Finally, the color code of the open stars indicates the values taken by the parameter let vary in each panel as appropriate and listed in the caption of Fig. 6.

In the middle panels of Fig. 6 we show what happens for single bursts of different age (five values are considered, namely 1, 2, 4, 7 8.5 Gyr) and constant fractionary mass (0.1 and 0.3 in the left and right panels respectively). In presence of a burst, the present-day stages (open stars) are bluer and brighter than the unperturbed case. This has important consequences for the Red Sequence and the Green Valley that depend on the fractionary mass of the bursts. The Red Sequence broadens towards bluer colors in presence either of massive and relatively young bursts (fractionary mass from 0.3 and larger and age equal or younger than 4 Gyr) or

less massive but very young burst (mass fraction lower than 0.20 and age younger than 2 Gyr).

In the bottom panels we replicate this analysis but now keeping fixed the age of bursts. It is quite evident that youngest bursts of any per cent mass can already take into account the great dispersion discussed in Section 2. Bursts with an age of 2 Gyr lead to final values that are not so different with respect to the unperturbed case: therefore, motivated by what we found in the upper panels for 7 Gyr-old bursts and in the middle panels for the green open stars, it is reasonable to say that bursts with age equal or older than, say, 4 Gyr do not lead to substantial variations on the CMD.

Finally, recalling the absence of α -enhancement for these experiments, it can be easily foreseen that taking it into account would likely lead to a broader dispersion on the evolutionary path of SSP-galaxies and a larger one in the $B - V$ color.

Mergers. In the above cases, dealing with bursts implicitly leads to assume that the seed galaxy is older than the burst component. From a cosmological point of view, a bound DM halo arises when the density peak height becomes greater than the local value (e.g. Press & Schechter 1974; Bond et al. 1991; Sheth & Tormen 2002), therefore, a galaxy can form inside a DM halo when the latter has accreted enough BM to ignite star formation. There is however a possibility that a galaxy will not survive for a long time because of cannibalism by other, more massive galaxies in its nearby surroundings: in this case, gas of the cannibalized galaxy becomes active fuel for the accretor. This latter in turn may be either older or younger than the former depending on the previous history. In such a case, photometric variations due both to stellar activity likely accompanying the merger and the stellar populations already in-situ are expected to happen. This means that together with a mix in ages, a mix in metallicity between different aged SSP-galaxies is also at work. Therefore, together with bursts mergers are expected to drive the dispersion on the CMD, especially inside galaxy clusters.

The situation is shown in Fig. 7: the cyan shaded area represents galaxies inside the WINGS clusters (total number of objects $N_{Tot} = 2325$), whereas the red squares are random mergers between SSP-galaxies. On the area populated by the observations we also show the contours of constant relative number of galaxies per elementary area of the CMD, $n(area)/N_{Tot}$, that is defined by $\Delta M_V = 1.0 \text{ mag} \times \Delta(B - V) = 0.1 \text{ mag}$. For the sake of comparison we plot the fiducial CMR of Sect. 2. Finally, the dashed vertical line is the limit for the faintest object in this dataset.

Using the sole merger hypothesis (left panel of Fig. 7), the dispersion would be even much larger than that of the bursts and, in particular, the simulations would extend also to the very blue and bright regions of the CMD. In contrast, these regions are avoided by real

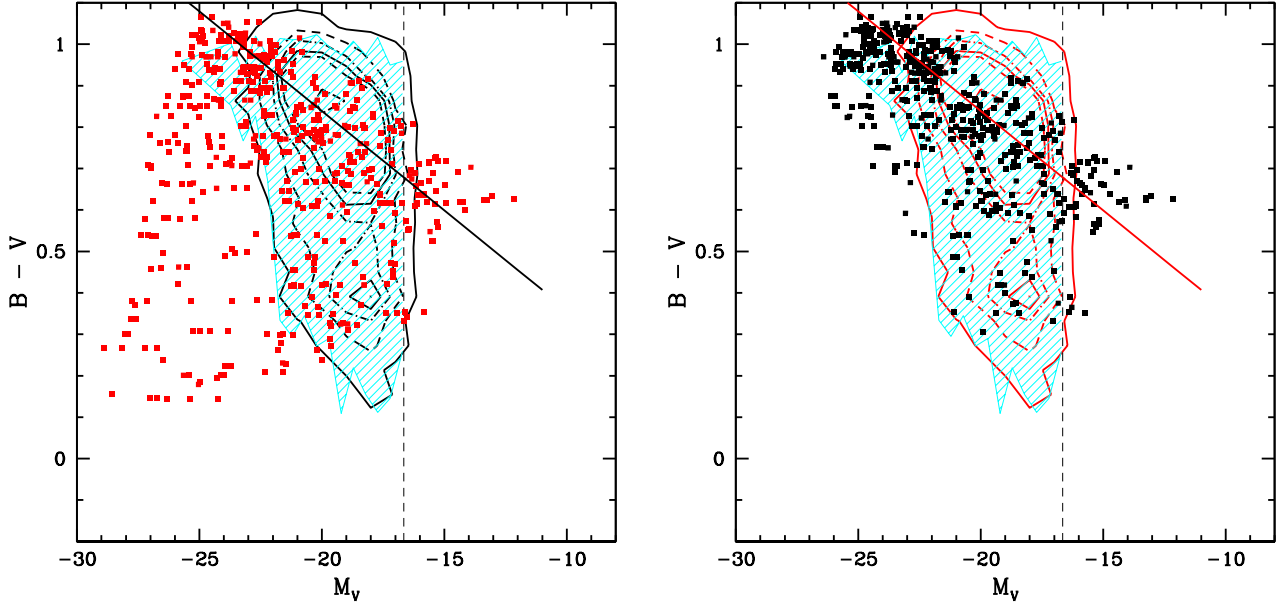


Figure 7. Left Panel: Simulation of 500 SSP-galaxies (red squares) with $T_{G,max} = 13$ Gyr, which underwent a single merger, observed at $z = 0$. Right Panel: Black squares represent other 500 SSP-galaxies simulated with the heuristic filter (the funnel); the black lines delimit the range in $B - V$ covered by the theoretical simulations with $\Delta M_V = 0.5$. In both panels the WINGS data for the sample of ten clusters (cyan shaded area) are shown for comparison together with the contours of constant relative number of galaxies per elementary area of the CMD, $n(area)/N_{Tot}$. The elementary area is $\Delta M_V = 1.0$ mag $\times \Delta(B - V) = 0.05$ mag. $N_{Tot} = 2325$ objects. The contour lines are for $n/N_{Tot} = 0.001, 0.005, 0.01, 0.015, 0.020, 0.050$, moving from the most external one, respectively. In both plots we display the fiducial CMR of Sect. 2 (black line in the left panel, red line in the right panel). Finally, the dashed vertical line is the limit for the faintest object in this dataset.

galaxies (this behavior has also been found in the case of bursts). This implies that a sort of selection rule must be at play, evidently breaking randomness and forcing real galaxies to avoid the region at the bright side of the Green Valley and the Blue Cloud. This is the photometric counterpart of the long known galaxy formation bias first pointed out by Kaiser (1984). At increasing mass of the collapsing over-density generating a galaxy of larger mass or even the cluster itself, clumps of matter that already collapsed (and hence formed stars) at previous epochs (higher redshifts) are already there. In other words high mass objects are very unlikely to be present in the remote past. Therefore a mere random process for mergers cannot be at work.

In order to take this into account in our simulations, we follow a heuristic simple reasoning: we just suppose that the range of ages admitted for each bin of galaxy masses gets narrower at increasing mass; this is equal to say that, instead of simulating encounters between galaxies of purely random ages, we apply a funnel in order to avoid formation of massive galaxies at recent times. As a consequence, also mergers among galaxies of comparable high mass are avoided. The funnel is represented by the factor f_M :

$$f_{M,i} = f_2 - (f_2 - f_1) \frac{M_{max} - M_i}{M_{max} - M_{min}} \quad (21)$$

where M_i is the logarithmic mass of the i -th galaxy, $i = 1, \dots, N$ and N is the total number of simulated galaxies, $M_{min} = 6$, $M_{max} = 13$ (the logarithm of the minimum and maximum galaxy mass in solar units we have adopted), $f_1 = 1$, $f_2 = 0.3$. Eqn. (20) then becomes:

$$t_{G,j} = t_{G,max,j} - f_M r t_{G,max,j}. \quad (22)$$

There are a number of reasons motivating this choice. First of all, massive galaxies are known to have their in-situ star formation already completed at $z = 1$ (e.g. Bower et al. 2006; De Lucia et al. 2006): as a consequence, an evolved massive galaxy cannot likely merge with a young counterpart of comparable mass, simply because there is a very small number, actually none, of such objects around. Second, at any redshift (leaving redshifts above say 10 aside) the number density per Mpc^3 of galaxies with mass in the interval 10^{10} to $10^{12} M_\odot$ is down by a factor from 10^5 to 10^8 or even more with respect to those in the mass interval 10^7 to $10^9 M_\odot$ (see Table 2 in Chiosi et al. 2017). This means that high mass galaxies merge only with smaller objects, with a probability increasing with decreasing mass of the latter ones. All this is mimicked by the factor f_M in the eqn. (22) above.

In the right panel of Fig. 7 we show the result of our funnel scheme: the galaxies, indicated by black squares, occupy the region delimited by black lines, spread in the CMD over more than 5 orders of magnitude in the V-band luminosity, and seem to agree with the observations much more than the red filled squares of the left panel. In particular a Red Sequence is clearly present and a “zone of exclusion” is in place. The funnel mechanism is effective in keeping massive galaxies out of the left side of the Green Valley, i.e. the lower side of the Red Sequence in this range of luminosities, in fair agreement with observational data. Furthermore, a better bounded Green Valley both in magnitude and colors is also produced by our simulations, and the bluest region of the WINGS dataset begins to be populated, too. Recalling the motivations for the funnel mechanism and the experiments shown in Fig. 6, this implies that we do not observe massive galaxies containing significant percentages of young stellar populations; in other words, the great bulk of stars in most luminous galaxies are old and red. The black dots are therefore demonstrating that, even with our over-simplified description of the merger history of a galaxy (reduced here to a single event), the heuristic funnel mechanism can confine galaxies in regions fully compatible with the observational data.

We also remark that, at variance with Fig. 5, a relatively small fraction of galaxies with $M_V < -22$ may reach $B - V > 1$: this result is consistent with the fact that (i) bursts add bulks of young stars which means bluer colors, whereas mergers always constitute a mix of gas (and likely young stars) and already existing old stars which implies redder colors; (ii) at low redshifts, when the “cosmic noon” i.e. the peak of the SFRD(z) has already occurred (see e.g. Fig. 9 of Madau & Dickinson 2014), dry mergers are more probable than the wet ones so that an already old ex-situ stellar component is more probable to be added to a seed galaxy; (iii) simulated bursts of reasonable intensity are never strong enough to parallel the effect of a whole galaxy; (iv) the simulations shown in Fig. 6 tell us that only perturbations due to very differently aged stellar populations may sensibly affect the B and V emissions; (v) in the case of mergers, a more realistic mix of metallicities is also present, so that a broad and adequately steep Red Sequence can form.

We conclude this section by remarking that single events of rejuvenation of stellar populations already effectively account for the dispersion in the region of star-forming galaxies, namely the whole Green Valley and the redder part of the Blue Cloud. One can easily foresee that: (i) If galaxies (let us consider intermediate masses only, so that a straight comparison with data is possible) containing significant populations of young stars are considered, we should find many more objects falling in the Blue Cloud. Adding young stellar populations to oldish galaxies shift them towards bluer colors and brighter magnitudes than the starting values. (ii)

An arbitrary mix of bursts and mergers is expected to affect the B and V fluxes more efficiently than single events. Starting from this reasoning, the Blue Cloud can be identified as the locus of the CMD occupied by galaxies containing just newly born stars independently of the age of “their seed” object; shortly speaking, independently of the age (redshift) at which the baryonic history of the galaxy began.

5. USING MODEL GALAXIES

The key result of the previous analysis is the suggestion that galaxies may scatter in the CMDs due to several causes such as age, chemical composition (metallicity), bursts of stellar activity, and mergers. However, the correct analysis of all these issues should rest on a suitable cosmological scenario describing the formation of galaxies inside a given volume of space (in other words a prescription for the formation and evolution of galaxies within a cluster) and models galaxies including their own histories of star formation and chemical enrichment. Two different strategies are possible that have already been successfully applied in cosmological context. The first one is the so-called merger branching-tree, in which DM halos and their baryonic content at each epoch are the result of previous mergers. Consequently, the number of branches increases with the redshift (see Lacey & Cole 1993, for a classical description): the main advantage of this is that mass growth of DM halos is easily followed up. The second one rests on the notion of the HMF, which is a suitable description (possibly analytical) of the number densities of DM halos as a function of mass and redshift in cosmological simulations. Although a detailed prescription of how DM potential wells evolve with time is missing in this approach, the HGF calculated from the HMF is nicely suited to our aims, because it allows us to explore the impact of cosmology in shaping CMDs with very little computational effort as compared to the detailed massive numerical simulations.

We build up our sample of galaxies inside a cluster in two steps: we first exploit the HMFs to get their relative HGFs, then using the MonteCarlo technique we randomly assign the formation redshifts z_f to all galaxies in the cluster respecting the mass-radius relation. Also in these simulations we will assume the Λ CDM concordance cosmology we have quoted above (namely $H_0 = 70.4 \text{ km s}^{-1} \text{ Mpc}^{-1}$, $\Omega_\Lambda = 0.73$, $\Omega_m = 0.27$, $\Omega_b = 0.05$, Komatsu et al. 2011).

The star formation and chemical enrichment histories of the member galaxies are described by suitable simple models that however are evolved in isolation (no mergers are allowed). Despite this major limitation, these galaxy models will prove to be good enough to provide a first description of the physical evolution of a cluster galaxy.

5.1. DM halos hosting BM galaxies

To get the population of DM halos hosting BM galaxies, we need to know how many halos of any given mass are inside a volume of arbitrary extension: to this aim, we apply the HGF formalism (Heitmann et al. 2006; Lukić et al. 2007) to obtain the comoving number density of DM halos as a function of redshift z . We briefly report here the definition of HGF, as the integral of HMF over a suitable range of masses $[M_1, M_2]$:

$$\begin{aligned} n(M_1, M_2, z) &= \int_{M_1}^{M_2} F(M, z) d \log M \\ &= \int_{M_1}^{M_2} \frac{dn}{d \log M} d \log M. \end{aligned} \quad (23)$$

The integrand, i.e. the HMF, contains three quantities that depend on the adopted cosmological scenario: the background density, $\rho_b(z)$; the variance of the linear density field, σ ; the fitting function, $f(\sigma)$; see the references above for all details. Via `HMFcalc`¹ (Murray et al. 2013) we get the values of HMF and sum them together inside mass bins centered at 10^7 , 10^8 , 10^9 , 10^{10} , 10^{11} , 10^{12} and $10^{13} M_\odot h^{-1}$ and wide $\Delta \log M = 0.4$.

The expression for eqn. (23) yields the *average* comoving number density of DM halos once fixed $f(\sigma)$, which is known to be tuned and to be varying from one cosmological simulation to another. Although it is easily predictable that varying the HMF will not change drastically the shaping of CMDs, we make use of `HMFcalc` to explore the effects of implementing different HMFs.

We then make use of this data to calculate simple 4-th order interpolating polynomials:

$$\log n(M_{DM,i}, z) = \sum_{j=0}^4 A_{i,j}(M_{DM,i}) \times z^j. \quad (24)$$

as made in Chiosi et al. (2012) and Chiosi et al. (2017); the i index relates the polynomial interpolation to each mass bin. In this way, we can easily incorporate the HGFs into generation of z_f for galaxies inside regions of Universe with desired values of radii (see Subsection 5.2).

The results of this analytical fit are shown in Fig. 8: the lines represent HGFs calculated inside the aforementioned mass bins, with labels indicating these latter, from the HMFs of Warren et al. (2006) (dashed lines), Angulo et al. (2012) (solid lines) and Behroozi et al. (2013) (dotted lines). The reader is also referred to Appendix B for further details about the coefficients of the polynomial fits. There are some differences between the curves of the same mass bin passing from a HMF to another, especially Angulo et al. (2012) who extend their fit to DM halo masses smaller than those considered by

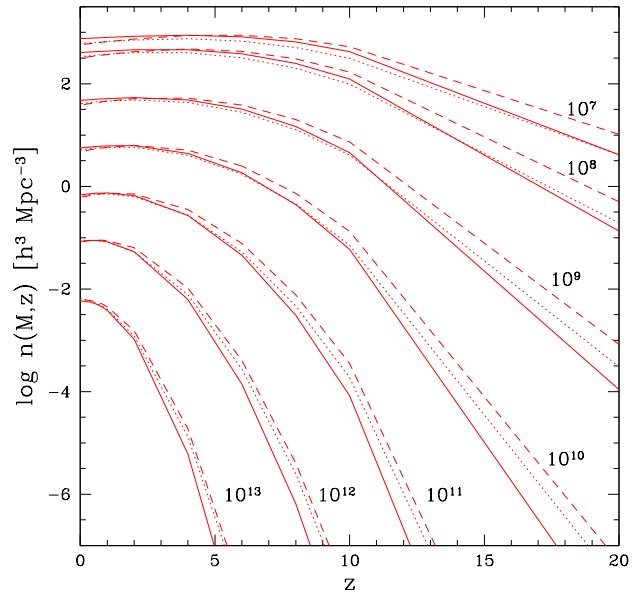


Figure 8. HGFs obtained from the HMFs of Warren et al. (2006) (dashed), Angulo et al. (2012) (solid) and Behroozi et al. (2013) (dotted). The curves are labeled with the values of the mass of the DM halos used to bin the HMFs. See the Appendix B for further details.

Warren et al. (2006) and Behroozi et al. (2013)². As already pointed out by Lukić et al. (2007), passing from a galaxy mass to another, each curve peaks at a different value of the redshift: this clearly shows that the HGFs already include the mergers among DM halos. However, the peak values of different HGFs are remarkably similar once fixed the mass bin: this just anticipates the fact that, like all average observables related to galaxies, the CMDs of clusters are statistically independent on the underlying precision cosmology.

Starting from Fig. 8, there are a few aspects of the HGFs worth being recalled: (i) the high merging efficiency leads all bins with $M \leq 10^{11} h^{-1} M_\odot$ to reach a peak at a value of z increasing with decreasing mass; (ii) the number densities of intermediate mass galaxies can both decrease by mergers and also grow because these galaxies are relatively deep potential wells; (iii) the number densities of the most massive halos ($M \geq 10^{12} h^{-1} M_\odot$) in the recent past keep on being constant or even increasing, because massive galaxies take long time to *become massive* by accreting DM and BM.

5.2. Galaxy Demography

² Further details about the mass range of best-fits for the three HMFs can be found in the cited papers or at the URL http://hmf.icrar.org/static/fitting_function_table/fitting_functions.pdf

¹ <http://hmf.icrar.org/>

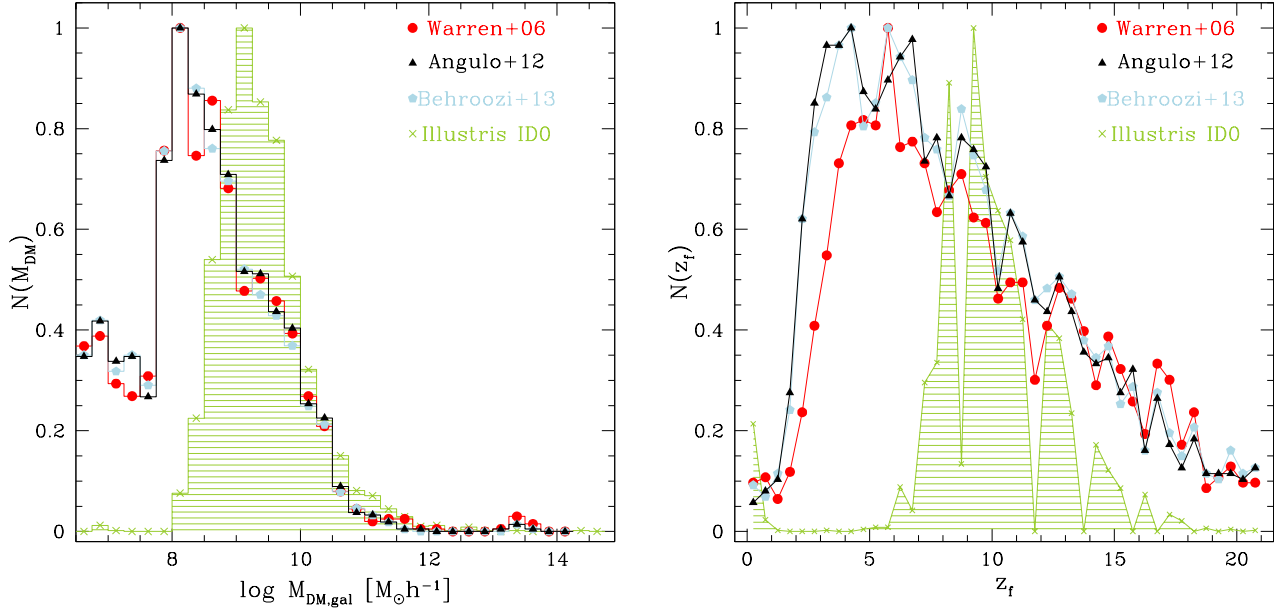


Figure 9. Comparison of demography of DM halos hosting galaxies inside clusters at $z = 0$ between ILLUSTRIS simulation (Vogelsberger et al. 2014, olive green crosses and shaded regions) and our random formation redshift generator using the three different HMFs: red dots are Warren et al. (2006), black triangles are Angulo et al. (2012) and light blue pentagons are Behroozi et al. (2013). In both sides, each histogram is normalized to the maximum value (see Table 4 and the text for more details). Left Panel: histograms of masses. Right Panel: histograms of z_f .

The HGF can now be used to generate galaxies hosted by DM halos with random masses and formation redshifts z_f . The cosmological limit imposed by the HGF is coupled with the mass-radius relation of galaxies, as already done by Chiosi et al. (2012) whose procedure is shortly summarized here.

The comoving number density $n(M_{DM}, z)$ is the result of two competing effects: the formation of new halos of mass M_{DM} via merger and/or acquisition of lower mass halos, and the destruction of halos of mass M_{DM} because they merge to form higher mass halos. Therefore, the following equation can be written

$$n(M_{DM}, z) = n(M_{DM}, z + \Delta z) + n_+(M_{DM}, z) - n_-(M_{DM}, z + \Delta z) \quad (25)$$

where n_+ and n_- represent the creation and destruction mechanisms. In particular, the quantity we are interested in is $n_+(M_{DM}, z)$, which is the number of new halos of mass M_{DM} which are born at redshift z .

The number of halos that merge to form higher mass systems is in turn a fraction of the number of halos existing at that time, i.e. $n_-(M_{DM}, z + \Delta z) = \eta_h \times n(M_{DM}, z + \Delta z)$, with $0 < \eta_h < 1$; so

$$n(M_{DM}, z) = n(M_{DM}, z + \Delta z) + n_+(M_{DM}, z) - \eta_h \times n(M_{DM}, z + \Delta z) \quad (26)$$

and

$$n_+(M_{DM}, z) = n(M_{DM}, z) - (1 - \eta_h) \times n(M_{DM}, z + \Delta z) \quad (27)$$

The only free parameter here is η_h , the fraction of halos that merge to form higher mass systems in the redshift interval $\Delta z = 0.145 \times z + 0.1$. In principle, the fraction η_h could vary with the redshift. However, for the sake of simplicity we assume that η_h remains constant and equal to 0.01 (see Chiosi et al. 2012, for details). For each interval $M_{DM}, M_{DM} + \Delta M_{DM}$ and $z, z + \Delta z$ we obtain a value $n_+(M_{DM}, z)$. This number, renormalized to unit over the whole redshift interval, can be considered as the *relative cumulative probability* that a halo of mass M_{DM} is born at redshift z .

Finally, for each halo of mass M_{DM} we compare a randomly chosen number $q \in (0, 1)$ with the cumulative probability

$$P_{z_i} = \sum_{z=z_{max}}^{z=z_i} n_+(M_{DM}, z) \quad (28)$$

until we have $q < P_{z_i}$, and take $z_f = z_i$ as its formation redshift; here z_{max} , which is the maximum redshift at which a DM halo hosting a galaxy observed at $z = 0$ starts to aggregate, is fixed to 21. It is worth recalling that after re-normalization the cumulative probability P_{z_i} is also confined in the interval $[0, 1]$. We then com-

Table 4. Number of simulated galaxies at $z = 0$ for two typical values of cluster radii and each HGF. The acronyms W06, A12, and B13 stand for Warren et al. (2006), Angulo et al. (2012), and Behroozi et al. (2013), respectively.

R_c [Mpc]	N_{W06}	N_{A12}	N_{B13}
1.25	1656	1789	1796
1.50	1883	2016	2033

bine the values of z_f of all galaxies with their values of M_{DM} , using the relationship by Fan et al. (2010)

$$R_{1/2} = 0.9 \frac{S_S(n)}{0.34} \frac{25}{m} \left(\frac{1.5}{f_*} \right)^2 \left(\frac{M_{DM}}{10^{12} M_\odot} \right)^{1/3} \frac{4}{(1+z_f)}. \quad (29)$$

which substantially links the stellar half-mass radius to the mass of its DM halo host. Here, $m = M_{DM}/M_*$ with M_* the stellar mass, $S_S(n_S)$ is a coefficient related to the Sersic indexes n_S and to the ansatz $R_{1/2} = S_S(n_S)R_g$ relating gravitational and stellar mass radii, f_* the velocity dispersion of the stellar component with respect to that of DM. For simplicity, we fix these quantities as $m = 10$, $S_S(n_S) = 0.34$, $f_* = 1$ (see Fan et al. 2010, for details).

With this procedure, we derive the populations of galaxies hosted DM halos that would be expected at $z = 0$ in ideal clusters with typical dimensions, namely with radii $R_c = 1.25$ and 1.5 Mpc. The total numbers of galaxies per cluster are listed in Table 4. We present our samples by examining the histograms of masses and z_f of DM halos hosting galaxies at $z = 0$. Both curves are normalized to the maximum value. Our predictions are compared with the most massive galaxy cluster found inside the ILLUSTRIS-1 simulation (Vogelsberger et al. 2014; Nelson et al. 2015), which is the most detailed, full physics simulation in their suite³. The comparison is shown in Fig. 9. We briefly recall that in ILLUSTRIS-1 the resolution in DM is $6.26 \times 10^6 M_\odot$ and the least massive DM friend of friends (FoF) must have 32 particles to be identified as a halo; the most massive galaxy cluster has a virial mass of $M_{200,mean} = 2.89 \times 10^{14} h^{-1} M_\odot$ and a virial radius of $R_{200,mean} = 1.66 h^{-1}$ Mpc, with the subscript indicating quantities evaluated inside the region having $\rho = 200 \times \langle \rho \rangle$, with $\langle \rho \rangle$ the mean density of the Universe. The sample analyzed here is made of only those DM halos hosting a non-zero stellar component, i.e. for which photometric data (magnitudes and colors) are given. The comparison is thus made with our synthetic clusters with physical radius $R_c = 1.25$ Mpc.

In the left panel, we see the distributions in mass for DM halos hosting BM galaxies. It is clear that the two prescriptions lead to distributions peaking at different values: we argue that this might be due to dynamical phenomena acting inside the ILLUSTRIS-1 cosmological box, e.g. mergers, shifting the peak towards higher masses, and tidal disruption, removing low mass DM halos. It is however interesting to note that both distributions resemble by eye some kind of a skewed Gaussian. In the right panel, we show the distributions of the same galaxies as a function of z_f . Here our samples are very different from those of ILLUSTRIS-1. Our galaxies broadly peak at $3 < z < 6$, with the bulk of objects already born earlier and a small number of them forming later. Inside ILLUSTRIS-1 the birth of galaxies, once reached a peak in frequency at $z \simeq 9$ [$t_{lb} \sim 13.2$ Gyr in terms of look-back time], is afterwards suppressed almost completely, with minor oscillations around 0 for $1 \lesssim z \lesssim 6$ and a final uprise at very recent epochs. Consequently, the ILLUSTRIS-1 sample is apparently missing galaxies born at intermediate redshifts [$7.8 \lesssim t_{lb}(\text{Gyr}) \lesssim 12.8$ in terms of look-back time], whereas in the same time interval our model does predict the formation of galaxies.

The large differences noted in Fig. 9 are surely related to the different approximations underlying both the complex hydrodynamical simulations of ILLUSTRIS-1 and our simplified approach. As recently discussed by Chua et al. (2017), the distribution of non-collisional matter (i.e. stars and DM) can effectively cool down in the cores of galaxies formed in the ancient epochs, at variance with those born more recently: this provides them much better chance of survival, or at least stronger resilience against potentially disruptive interactions that they would surely undergo throughout the cluster environment. A key role is also played by the host cluster itself because the mass profile of this latter becomes steeper and steeper in the core because of dynamical relaxation, consequently the environment gets denser with time: this trend is found to be quantifiable in terms of the number of dynamical times elapsed since the cluster formation (e.g. Jiang & vandenBosch 2016). Therefore, each galaxy has to attain a sufficiently cold core in order firstly to survive in the cluster environment, and then to grow by accretion of matter from ICM and by mergers with other substructures. Given these preliminary considerations, which explain evaporation of galaxies while falling into more massive halos, the inclusion of the BM physics in this context is crucial and its effects are still not fully explored. Basing on a systematic comparison of the full-physics and dark-matter-only ILLUSTRIS suites, Chua et al. (2017) claim that galactic winds and photo-ionization from UV radiation may effectively inhibits mass aggregation at least at the low-mass end and in certain regimes of redshifts (see also Despali & Vegetti 2017 for similar reasoning for DM subhalos of intermediate masses in-

³ <http://www.illustris-project.org/data/>

side ILLUSTRIS and EAGLE simulations, Schaye et al. 2015). In particular, photometric data inside ILLUSTRIS are bound to whether stellar particles, i.e. stellar populations, are found inside a bound sub-halo: recalling that in ILLUSTRIS-1 the average gas cell mass is $8.86 \times 10^5 M_{\odot}$, from which integrated stellar populations might stem, and that a prescription for subgrid physics is always needed to follow up integrated properties of all kind of particles, these could be a substantial limit of state-of-art hydrodynamical simulations in describing photometry, especially for galaxies inside more recently formed DM halos of lower masses. On the other side, our numerical approach, at the basis of the build-up of samples inside clusters, provides a population of galaxies which should reflect the observational evidence of the mass-radius relation at $z \sim 0$ (Chiosi et al. 2012): if observed galaxies are merely those which survived to all disrupting interactions they underwent, then at least a minimum fraction of the sample (not as close to zero as the one of ILLUSTRIS-1) should have formed in an evidently large range of look-back time. However, acknowledging that our approach might not be the most refined one, we feel that the best interpretation might be a middle ground between the two models.

Summing up, as seen in Section 4.1, especially in Figures 5 and 7, dispersion inside CMDs is driven by scatter in formation epochs: we can say that our model, although crude and not closely resembling cosmological simulations, is still fully adequate in locating the birth of galaxies in cosmic epochs. Moreover, distributions built up from HGFs are evidently very similar in terms of both masses and z_f , with the only slight exception of the formation redshifts arising from Warren et al. (2006) that peak about 2 Gyr earlier than those of the other two distributions. As it will better proved in Appendix B and anticipating here the results displayed in Fig. 10, we argue that when the integrated properties of single galaxies are analyzed, such as light emitted as a whole, typical informations on precision cosmology like for instance cosmological parameters or mass resolution are almost completely lost.

5.3. Path of model galaxies on the CMD: comparison with data

In Fig. 10 we show the CMD of galaxies inside the reference cluster (radius: 1.50 Mpc; underlying HGF: Warren et al. 2006). The left panel shows galaxy models with no galactic wind, whereas the right panel those with galactic winds. In view of the discussion below it is worth recalling here that the integrated spectra of the models galaxies, albeit in a very simple way, take the effects of interstellar dust into account. Moreover the simulated galaxy content of clusters does not consider the geometric structure of the cluster as far as the star formation, metal enrichment, and photometric histories of the component galaxies and their position within a given clusters are concerned.

Prior to any other consideration, we need to shortly describe the path of a model galaxy on the CMD. In both panels the generic path is indicated by a red solid line. Each path corresponds to a galaxy of different total mass as indicated in Table 2. Starting from the bottom (the early stages of a galaxy's evolutionary history) the stellar mass emitting the light is low and the metallicity is low as well. As time proceeds, the stellar mass and the metallicity reached by the gas increase. In other words, the stellar mass is a mixture of many generations of stars of different age and metallicity each of these contributing to the total light. The contributions are in turn weighed by the star formation rate at the time of formation. The integrated light whose intensity and color determines the position on the CMD. Since the luminous star mass first increases and later decreases because stars either explode as SNaE or leave faint remnants that do not contribute to the light, the path on the CMD first goes towards more negative magnitudes and then bends over to less luminous magnitudes. In the meantime the colors become redder and redder both because of increasing metallicity and aging of the already existing evolving stars. This trend is however contrasted by newly born stellar generations by the effect of the bright, blue massive stars, i.e. in presence of active star formation. It goes without saying that, as gas is used up by star formation, this latter effect tends to decrease and eventually disappear when star formation ceases completely. Furthermore we like to comment that the mean metallicity reached by any galaxy affects its location on the red sequence both in absence and presence of galactic winds. Last point to note is that the dashed line in both panels of Fig. 10 connect stages of equal age in the rest-frame of the model galaxies. From bottom to top the age goes from 1 to 13 Gyr, in steps of 1 Gyr.

We plot also the data of the ten best WINGS clusters (cyan points) and the most massive galaxy cluster inside ILLUSTRIS-1 simulation (green shaded area). Both the WINGS data and the ILLUSTRIS-1 simulations show the well known drop-off towards the Green Valley and the Blue Cloud (see Nelson et al. 2018, and references therein). Roughly speaking, the Green Valley is confined in the color range $0.6 < B - V < 0.8$, has nearly the same slope of the Red Sequence and is populated by fewer objects. Finally the Blue Cloud, customarily associated to galaxies with ongoing star formation (e.g. spirals and robust dwarfs), falls below the Green Valley and has a numerous population. The relatively scarce population of the Green Valley may suggest that galaxies are either slowly accelerating their evolution but still retain some residual stellar activity (left panel of Fig. 10) or past the major star forming activity and the sudden interruption of this by galactic wind quickly evolve toward the region of red colors (right panel of Fig. 10). The alternative depends of the true relative number of galaxies in the three regions that is subject to complete-

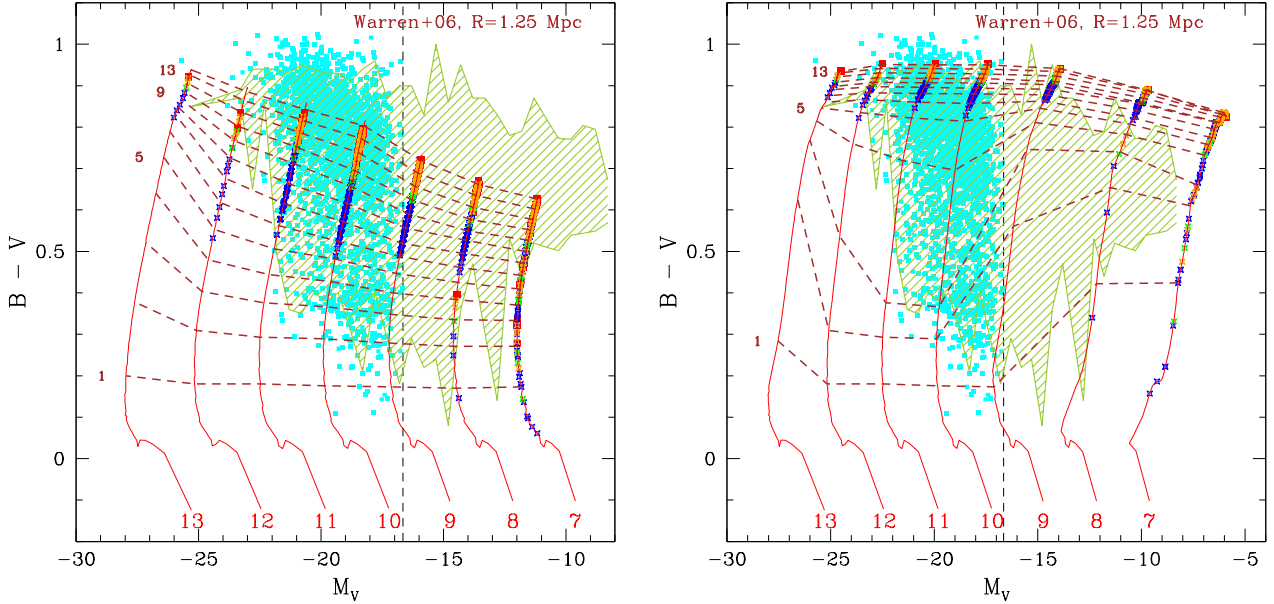


Figure 10. CMD of galaxies for the reference cluster (see text for details). The green shaded area represents galaxies of the most massive cluster inside ILLUSTRIS-1 simulation; the cyan points are galaxies of the selected sample of the WINGS clusters. The vertical dashed line indicates the limit of the faintest object; the red solid lines are the evolutionary paths in the rest frame of the model galaxies of different baryonic mass, from 10^7 (right) to $10^{13} M_{\odot}$ (left) in steps of a factor of ten. The value of the mass (on logarithmic scale and in solar units) is also indicated along each line. Open stars along the lines are selected stages of the model galaxies as they would be observed at various bins of redshifts (at decreasing redshift, blue is for $0.1 < z \leq 0.5$, green for $0.05 < z \leq 0.1$, orange for $0.01 < z \leq 0.05$, red for $z \sim 0$). The dark red dashed lines connect the stages of equal age for each mass, with time steps of 1 Gyr from 1 to 13 Gyr from bottom to top. Ages in Gyr are also indicated along the dashed lines limited to a few cases for the sake of clarity. **Left Panel:** models with modulated star formation. **Right Panel:** models with straight galactic wind.

ness of the observational data. Assessing this issue is beyond the aims of the present study.

Looking at the left panel, in which no galactic winds are considered, a number of features are evident. First of all, all evolutionary paths (the red solid lines) end up at $B - V$'s that increase with the galaxy mass: thus defining the locus in the CMD of the present-day stage. However, it is worth noting that along this line, star formation is still going on albeit at minimal levels does (see the blue solid lines in Fig. 4 showing the SFR vs age relationship for this type of galaxy models). The slope of the constant age loci (dashed lines in Fig 10) becomes more and more negative at increasing age. Both the location and slope of the present-age stages nearly coincide with the location of the bulk galaxies along the observational Red Sequence (by eye inspection the theoretical slope is half the observed one), thus providing a simple and consistent way of explaining the CMR.

However, looking at the slopes of the different datasets in their most dense regions, we see that our end-point line falls in between those for the WINGS and the ILLUSTRIS-1 clusters, the slopes of which are steeper and flatter, respectively.

However, we clearly see that a $\Delta(B - V) \sim 0.6$ and $\Delta M_V \sim 6$ -wide region of WINGS and ILLUSTRIS-1 data, containing the star forming galaxies, requires that other mechanisms must be taken into account to get their much bluer colors: these are mainly bursts and mergers, the effects of which have already been anticipated with the aid of the SSPs-galaxies.

In the right panel we briefly show the consequences of applying galactic winds to our model galaxies: we proceed as in Tantaló et al. (1996, 1998) and Chiosi et al. (2017), who stop the star formation process when the energy injection by supernova explosions and stellar winds overwhelms the efficiency of radiative cooling and the internal energy of the gas exceeds the gravitational energy of this. Therefore, the gas is supposed to leave the galaxy in form of galactic winds and subsequently the galaxy to evolve passively. Since star formation has ceased, galaxies quickly become red and as the evolution proceeds they get redder and redder but at slower pace. Consequently, after the onset of galactic winds the lines of constant age on the CMD are first squeezed in a narrow color range but also run much flatter than in the previous case. In the CMD, all galaxies but for those of the lowest mass stack along a locus of very red colors

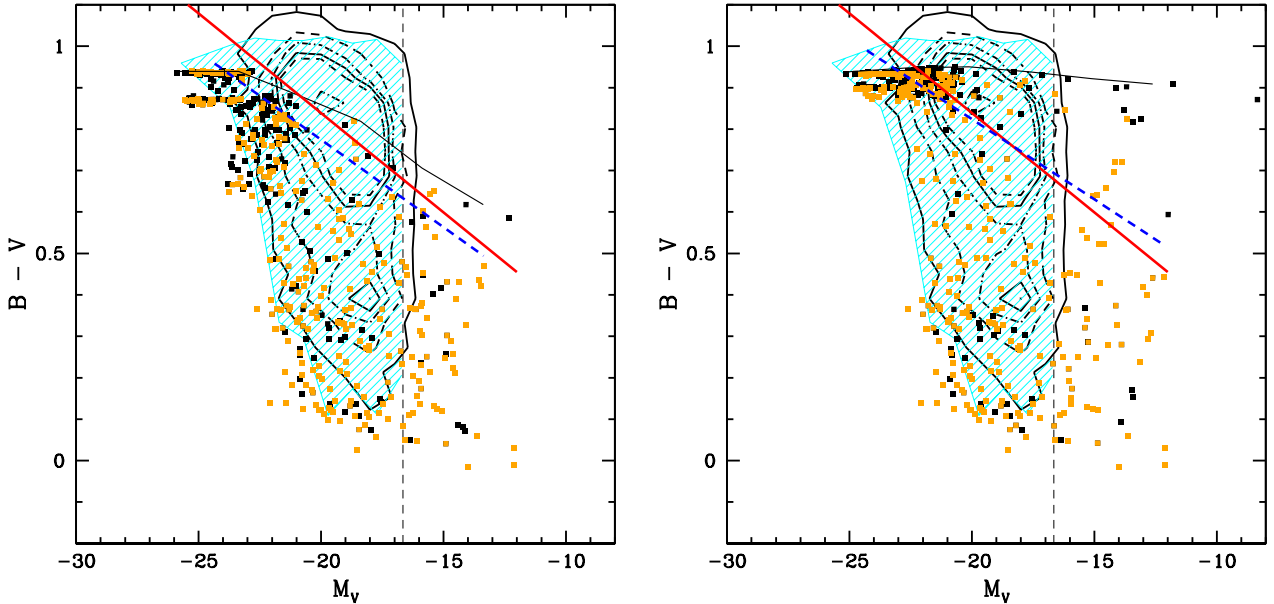


Figure 11. Galaxy mergers. Left Panel: the case of galaxy models with modulated star formation; black squares are the mergers of two early-type galaxies ($ET_{ms}+ET_{ms}$). Yellow squares are either the mergers of two late-type objects ($LT_{ms}+LT_{ms}$) or of a late-type plus an early-type galaxy ($ET_{ms}+LT_{ms}$). The underlying HGF is the one by Warren et al. (2006). Right Panel: the same as in left panel but early-type galaxy models now considered have straight galactic wind, ET_{gw} . Note the different upper boundary at red $B-V$ colors. In both panels, the shaded area shows the data for the selected sample of WINGS clusters together with the contour lines of constant fractionary number of galaxies per elementary area of the CMD already presented in Fig. 7, the fiducial CMR of Sect. 2 (thick red line in the left panel, and thick black line in the right panel), and the best fit of the model galaxies falling within the 1σ uncertainty strip of the fiducial CMR (the dashed lines). See the text for more details.

confined in the interval $0.8 < B-V < 1$ for magnitudes in the range $-12 > M_V > -25$. In this case the theoretical Red Sequence runs flatter than in the previous case and fails to match the bulk red galaxies.

The two ridge lines of the reddest colors in both panels of Fig. 10 can be thought as a sort of theoretical boundaries for the Red Sequence (locus of $z = 0$, hence maximum age for galaxies on the CMD). In other words the reddest models in both panels highlight the region of uncertainty or natural thickness of the Red Sequence due to the existence of galactic winds, or in a more general way the existence of competing and contrasting effects caused by gas heating by energy injection, gas cooling by radiative processes, and gas trapping by gravitation. Since the interplay among all these factors likely varies from a galaxy to another, this may easily be an additional source of large dispersion along the Red Sequence towards the reddest colors.

Basing on the results of this simple analysis of the effects engendered by galactic winds, we may perhaps suggest that (i) galactic winds do not proceed according to the simple mechanism envisioned by Larson (1974), sudden ejection of all gas from the whole galaxy, but rather a local loss of hot gas over a certain time while star formation in other regions of the same galaxy may still be under way (as indicated by NB-TSPH models of

Merlin & Chiosi 2006, 2007; Merlin et al. 2012). Therefore in real galaxies all situations encompassed by the two paradigmatic cases are possible. Despite the presence of galactic winds, galaxies may still retain some gas and continue to form stars. (ii) Since in models with sudden galactic winds the lines of constant age from 13 to 4 Gyr are squeezed in a narrow range of red colors, they cannot account for the large dispersion of colors towards the blue side of in the CMD. Therefore there must be other concomitant causes at work, chief among them is dispersion in the galaxy formation redshift z_f soon after which the dominant star forming episode occurs. In this sense galactic winds are a *secondary process* with respect to the dispersion in z_f and rejuvenation of stellar populations. In alternative, one could also consider the effects of the dynamical interaction of a galaxy with the environment on star formation and AGN fueling. Gas could be stripped from a galaxy by ram pressure, harassment, and mergers (see Silk & Mamon 2012, for a recent review on galaxy formation and evolution).

5.3.1. More realistic CMDs for merging galaxies

The last step of our analysis is to generate CMDs simulating mergers of galaxies with different ages and masses. The galaxy models incorporate a realistic description of the star formation and metal enrichment

histories and also the occurrence of galactic winds following the energy feedback by supernova explosions and stellar winds. Ages and masses of model galaxies to be merged are chosen by means of the Monte-Carlo procedure, but the relative occurrence probability of each mass with respect to the whole permitted mass spectrum is modulated by the HGF of DM halos at each redshift (that by construction contains the physics expressed by the “funnel” condition).

The procedure is as follows: we randomly choose a mass in $[M_L, M_U]$ and then use its own photometric history in the rest-frame to place the object on the CMD; in the space $n(M, z)$ we determine the halo number density of the HGF which upon normalization is used as a probability of occurrence and replaces the factor f_M in eqn. (22).

In other words, we are repeating the experiments of Section 4 using the galaxy models of type ET_{ms} (modulated star formation) and ET_{gw} (sudden galactic wind) instead of the SSP-galaxies. We remind the reader that the galaxy models are those already shown in the two panels of Fig.10 (the red solid lines), whereas the SSP-galaxies are those already shown in Fig. 6 (black dotted lines). We also make use of the LT_{ms} models (for the sake of simplicity, we do not plot their paths in the CMD).

In these simulations, the HGF which is customarily used as number density of halos, it is now recast as the occurrence probability of a halo of given mass and formation redshift z_f . This by construction replaces the funnel condition with its physically grounded counterpart.

Since all the three cosmological HGFs in usage are very similar each other (see Fig. 8), nearly identical results are to be expected adopting one or another HGF. Therefore we limit ourselves to show here the results for the sole HGF of Warren et al. (2006).

The results are plotted in Fig. 11, in which the left panel displays mergers among galaxies randomly chosen from the ET_{ms} and LT_{ms} groups and the right panel shows the same but now for groups ET_{gw} and LT_{ms} . The simulated CMDs nicely reproduce the WINGS data of Cariddi et al. (2018), i.e. the existence of the three loci in the CMD, i.e the Red Sequence, the Green Valley, and the blue Group, and may also account for the extended overlapping of early and late-type galaxies pointed out in Fig. 3. A remarkable crowding of points can be seen in the Blue Cloud, at variance with Fig. 7 in which only the reddest part was populated: this is essentially due to the broader temporal extension of the star forming activity (and hence bluer colors) in the model galaxies compared to the sharp assignment of ages to the bulk stellar populations of the merging SSP-galaxies. Interestingly this feature is visible in both panels: we already know that the Blue Cloud is the locus occupied by galaxies hosting very young stars, but this comparison tells us that the star formation activity is

Table 5. Age and redshift variation of the theoretical CMR ($B - V$) = $A \cdot M_V + B$ from models ET_{ms} .

T_U (Gyr)	z	A	B	rms
13	0.06	-0.023	0.359	0.011
12	0.14	-0.023	0.329	0.011
11	0.23	-0.023	0.301	0.012
10	0.34	-0.022	0.282	0.012
9	0.46	-0.021	0.266	0.014
8	0.60	-0.019	0.263	0.012
7	0.78	-0.017	0.259	0.013
6	0.99	-0.014	0.262	0.011
5	1.27	-0.011	0.263	0.008
4	1.66	-0.009	0.261	0.006

truly at the peak with gas being converted into stars at maximum efficiency otherwise they would fall into the Green Valley. This latter being less populated than the Blue Cloud lends additional support to the notion that the Green Valley should correspond to a rather short evolutionary phase for galaxies. Finally, in both panels we see a large number of galaxies crowding the Red Sequence, The two panels also highlight a point that could be relevant in relation to the nature and mode in which galactic winds should occur. As a matter of facts, ET_{gw} and ET_{ms} models predict a different slope for the red boundary of the $B - V$ distribution, nearly flat the former, and close to the observational one (negative slope) the latter. The reddest colors for the two distributions agree with those of the observational one. The simple conclusion one might derive from this is that the Larson (1974) model of galactic winds does not find correspondence in what implied by the observational data. This suggestion is not new because it has been pointed out several times (see for instance Chiosi et al. 1998; Chiosi & Carraro 2002; Merlin et al. 2012), however it is also confirmed by the analysis of the CMDs derived from the integral B and V magnitudes of cluster galaxies. Insufficient correction for reddening by dust could be a reasonable way out and an alternative at the same time. However, the issue requires further investigation before drawing any conclusion.

5.3.2. The Red Sequence, Green Valley, and Blue Cloud

The evolutionary tracks of model galaxies in Fig. 10 (red lines) and their evolutionary rate along these paths (the stages marked with different symbols according to the considered redshift interval) clearly show that depending on the galaxy mass and mean metallicity, and the complicated physics of the galactic gas, various cases are possible.

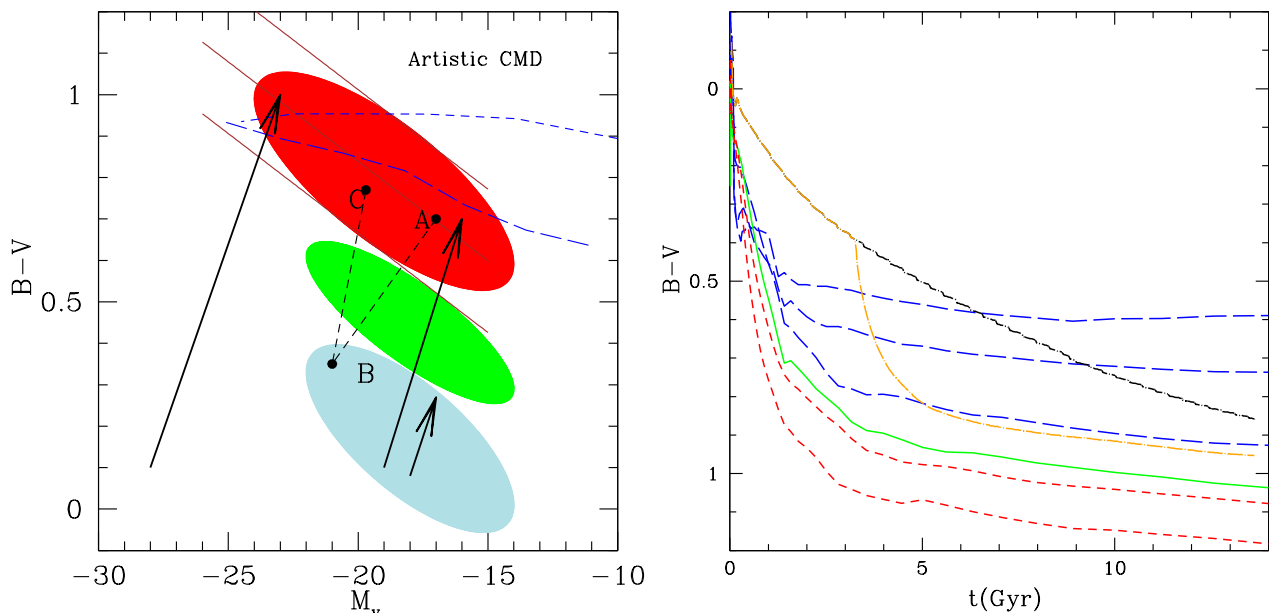


Figure 12. Left Panel: Artistic view of the Red Sequence, Green Valley and Blue Cloud on the CMD of real galaxies. Superposed are three schematic evolutionary sequences of model galaxies with different mass (black arrows), the terminal stage at $z = 0$ both in absence (long-dashed blue line) and presence of galactic wind (short-dashed blue line). Schematically we also show the path of a red old galaxy (point A) undergoing a transient burst of star formation either by internal or external (merger) causes (dotted line, point B), and nearly recovering the original position (point C). Right Panel: the evolutionary paths of SSPs and model galaxies in the Color vs Age plane. SSPs are grouped according to their metallicity: long-dashed blue for $0.001 \leq Z \leq 0.008$, solid green the solar case ($Z = 0.019$), and short-dashed red for $0.40 \leq Z \leq 0.070$). The galaxy models are ET_{ms} (dot short-dashed black) and ET_{gw} (dot short-dashed orange) of $10^{11} M_{\odot}$.

In view of the discussion below, in Fig. 12 we schematically show the Red Sequence, Green Valley, and Blue Cloud together with the evolutionary paths of galaxies on the CMD. Specifically, we draw the Red Sequence with inclination and thickness using the values quoted in Section 2. Let us shortly present the different cases as a function of the galaxy mass: (i) Galaxies in the mass interval $10^{13} > M > 10^{12} M_{\odot}$ can be found on the Red Sequence only. This means that today no galaxy with this mass can be seen in the Green Valley or Blue Cloud: ongoing star formation either in isolation or as consequence of mergers does no longer occur. (ii) Galaxies in the mass interval $10^{12} > M > 10^9 M_{\odot}$ can be in any of the three regions depending on their individual evolutionary history. If they evolve in isolation, at beginning when the star formation is very strong they populate the Blue Cloud, cross the Green Valley towards the end of the star forming activity they cross the Green Valley (fewer stars are formed and the stellar content gets older and redder), finally when the star formation activity extinguishes, they become old and red. If they undergo mergers when they are on the Red Sequence, they first fall either on the Green Valley or Blue Cloud depending on the intensity of the burst of star formation. For small bursts engaging a small fraction of the total star mass, when the burst is over the CMD galaxy may recover

the old position on the Red Sequence. In contrast, for mergers among objects of comparable mass but different ages, the burst is very intense, and afterwards the composed object can hardly recover the original position on the Red Sequence but remains bluer and brighter for very long times. (iii) Galaxies with masses in the interval $10^9 > M > 10^7 M_{\odot}$ are not present in the WINGS data because of the limit magnitude of the survey but they exist in the ILLUSTRIS-1 simulations, that in turn likely suffer of incompleteness due to numerical resolution in the mass interval $10^8 > M > 10^6 M_{\odot}$. Therefore the discussion of their evolution on the CMD is not of interest here.

The above considerations are supported and strengthened by the variation of $B - V$ color as a function of the age for both SSPs and model galaxies, shown in the right panel of Fig. 12. Here we display a few SSPs with different metallicity (blue for $0.001 \leq Z \leq 0.008$, green for the solar case $Z = 0.019$, and red for $0.40 \leq Z \leq 0.070$). We also show two galaxy models of the same mass, $10^{11} M_{\odot}$ but different evolutionary histories, namely ET_{ms} (yellow) and ET_{gw} (black). Both SSPs and galaxy models behave as expected: the SSPs are very blue when young massive stars are present; they get red as these latter disappear and when AGB first and RGB plus AGB stars are present; they get even redder on rather short

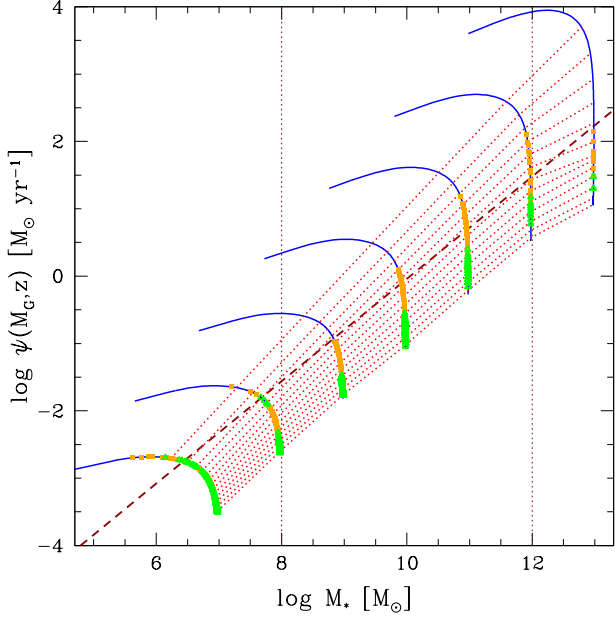


Figure 13. SFR versus Stellar Mass: the solid squares are model galaxies observed at $0.1 < z \leq 0.7$ (orange solid squares) and $z \leq 0.1$ (green open triangles); the blue solid lines are the evolutionary paths (from left to right) of each model galaxy; the dark-red dashed line represents the [Renzini & Peng \(2015\)](#) average relation for star-forming galaxies, which range of validity is identified by the two black dashed vertical lines; the red dotted lines connect points of same age for each mass, in time steps of 1 Gyr from 1 to 13 Gyr from top to bottom.

timescales (fast evolution on the CMD plane) because the RGB phase dominates the color evolution, and remain red at nearly constant color afterwards. The two model galaxies have a similar appearance at the older ages (namely older than 12 Gyr): they remain very blue as long as star formation is active, because massive young stars are present, and plunge to red colors after star formation ceases, with a rate depending on the strength of winds inside the galaxy itself.

5.4. Physical meaning and evolution of the CMR

The observational data show two distinct groupings of red galaxies: a first one made by those crowding along the Red Sequence with mean slope $A = -0.048$, and a second less numerous group whose (B-V) colors exceed the upper limit of the CMR itself and run nearly constant with the absolute magnitude (mass). Furthermore, among the brightest galaxies of both groups the colors become nearly independent of the luminosity (mass): the CMR flattens out.

The theoretical models also show a similar behavior that seems to depend on the interplay between star formation and galactic winds. The models (ET_{ms}) in which the energy feedback instead of energizing the galactic

wind goes into modulating (decreasing) the SFR, their present-day (B-V) colors run along a sequence whose slope (see the entries of Table 5) is comparable to the observational one of the first group above. In contrast, models (ET_{gw}) whose energy feedback straightly goes into the galactic wind, so that they suddenly extinguish star formation and evolve passively ever since, reach present-day (B-V) colors close to the limit values of the second group and remain nearly constant with the absolute magnitudes. Finally, for the brightest galaxies the colors seem to become constant at the mean value (B-V)=0.95 (see both panels of Fig.11), the typical value for luminous early type objects.

Furthermore, it is implicit that when galactic winds occur for whatever reason a galaxy switches from the first to the second group.

Finally, the constant (B-V) color of the most luminous galaxies could be attributed to a constant metallicity: the mass-metallicity sequence of the CMR breaks down for this type of galaxies, in agreement with recent observational data and theoretical NB-TSPH simulations (e.g. [Tremonti et al. 2004](#); [Mannucci et al. 2010](#); [Mannucci & Cresci 2012](#); [Cresci et al. 2012](#); [Bothwell et al. 2013](#); [Torrey et al. 2014, 2017](#); [Matsuoka et al. 2018](#), and references) and theoretical NB-TSPH simulations ([Chiosi & Carraro 2002](#); [Merlin & Chiosi 2006, 2007](#); [Merlin et al. 2012](#)).

The last interesting issue to address here is the time dependence of the CMR as function of the age. In both panels of Fig.10 the red dashed line visually show the CMR at different ages going from 13 Gyr (top) to 1 Gyr (bottom). While the CMR gradually varies from 1 Gyr to the present and the slope gently gets steeper with increasing age for galaxy models with no galactic winds, much more drastic changes occur in the presence of sudden galactic winds that usually set in early in the evolutionary history ($T_G \lesssim 4$ Gyr) of a galaxy. Past 4 Gyr the CMR is much more regular, uniform and nearly flat. This unlikely behavior of the CMR strongly suggest that the [Larson \(1974\)](#) mode of galactic wind is too a crude description of this phenomenon: therefore in the following we limit ourselves to the case of ET_{ms} models to discuss the time evolution of the CMR(t). In Table 5 for a few select value of the rest-frame galaxy ages, and galaxy masses from 10^7 to $10^{12} M_\odot$, and using a linear least-square fit of the data ($B - V = A \cdot M_V + B$) we derive the slope A , the zero-point B and the r.m.s. The slope remains nearly the same from 13 Gyr down to 8 Gyr ($z=0.6$), whereas in the age interval 8 to 4 ($z=1.66$) it goes down to nearly zero. To discuss the time dependence of the CMR with the observational data to our disposal is not possible. Because of the very small redshift coverage (e.g. $z=0.04$ to $z=0.07$ in [Cariddi et al. 2018](#)) and also because theoretical magnitudes and colors in other photometric systems and pass-bands would be required. Therefore we leave the subject to a future study. In any case, we would like to mention here that

starting from the rest-frame age of 6 Gyr, i.e. $z=0.99 \simeq 1$ the slope of the CMR is significantly different from zero and stable in agreement with observational data on high redshift objects (Gladders et al. 1998; Tran et al. 2007; Mei et al. 2009).

The conclusion one would draw from the above picture is that the inclination of the crowded Red Sequence implies that a minor residual stellar activity is at work or ceased in a very recent past. The upper boundary may be sensitive to the underlying mechanism of energy feed-back in driving galactic winds and regulating the efficiency of star formation and chemical enrichment. In other words the CMR in addition to being an indicator of mass-metallicity sequence is also the signature of the past star formation activity. Finally, looking at the Red Sequence sub-populations one could infer about the kind of star formation history of galaxies.

Before closing this section, we like to shortly comment on the potential of the CMR for cosmological studies. A great deal of observational data suggest that early-type galaxies are nearly coeval, had their last episode of intense star formation at high redshift ($z \geq 2$) and evolved nearly passively since then (see e.g. Bower et al. 1992c,b; Aragon-Salamanca et al. 1993; Pahre et al. 1996; van Dokkum et al. 1998; Stanford et al. 1998; Gladders et al. 1998; Chiosi 2002; Chiosi & Carraro 2002; Peebles 2002; Chiosi 2007; Chiosi et al. 2014). Consequently, the CMR can be in place at high redshift and thus be a great potential tool for cosmological studies (Sandage 1972). In particular, any change in its slope could signal changes in the star formation history (and/or metallicity). In this context, starting from previous work by Visvanathan & Sandage (1977), Sandage & Visvanathan (1978b,a), and Bower et al. (1992c,b), López-Cruz et al. (2004) addressed the question of the universality of the CMR in cluster early-type galaxies. Analyzing the CMR of 57 galaxy clusters of the Abell sample over the redshift interval $0.02 < z < 0.2$, they found that the CMR is linear over about eight magnitudes with no breaks in the slope, and that changes in the slope can be explained by metallicity and passive evolution. Furthermore, they pointed out that the CMR could be an accurate indicator of membership and redshift. We would like to note that the results presented in Figs. 10, 11, and 14 could be used for this kind of studies. However, this is beyond the aims of this study and is left to future investigation.

5.5. SFR vs Stellar Mass Relationship

We conclude the analysis of model galaxies by addressing the issue of the relation between SFR and stellar mass, vividly debated in literature (see e.g. Renzini & Peng 2015, and references therein). This gives also the possibility to show the underlying physics at work for model galaxies exploited until now in terms of photometry. Since one needs galaxies with ongoing star formation at the present time ($z = 0$) we

consider only galaxy models with no galactic winds, i.e. with residual star-forming activity. The theoretical SFR versus stellar mass relation is shown in Fig. 13. We schematically build it up as Fig. 10, because randomness of z_f plays a key role in shaping also this relation. The solid blue lines show the relations for galaxy models of increasing mass as indicated, whereas the dotted lines indicate loci of different ages in the rest-frame: we refer to these latter as the age grid. Finally, the dark red dashed line is the empirical mean relation by Renzini & Peng (2015) for star-forming galaxies in the SDSS DR7 sample spanning the redshift range $0.02 < z < 0.08$. To better compare the observational data for the SFR vs stellar mass relationship with our randomly-born model galaxies, for these latter we also plot the stages in the redshift interval $0 \leq z \leq 0.1$ (the green triangles).

An overall agreement with observations is evident: the slope of our synthetic dataset is nearly identical to that of the observational data or their best-fit relationship. However, the model galaxies at the ridge line for $z \leq 0.1$ are on average 0.5 dex below the Renzini & Peng (2015) relation. This means that either the model galaxies have a SFR 0.5 dex lower than observed or a stellar mass 0.5 dex larger than estimated for the observed galaxies or a suitable combination of the two effects. As far as the SFR is concerned, the one of the model galaxies in the redshift interval $0 \leq z \leq 0.1$ is already in the long tail following the peak value that occurred in the past. To evaluate the effect of it, we also plot the model galaxies as observed in the redshift interval $0.1 < z \leq 0.7$ (orange solid squares), which broadly corresponds to include galaxies at a look-back time of $7 \lesssim t_{lb}(\text{Gyr}) \lesssim 12.5$: by including these younger and gas-richer galaxies, the Renzini & Peng (2015) relation is fully recovered. We remark that the case of model galaxies with the Larson (1974) scheme for galactic wind cannot be plotted in this diagram, because their present-day SFR would be zero. However keeping mind that in real galaxies the galactic winds seem to occur any time a fraction of gas may be hot enough to acquire enough kinetic energy to escape the galaxy, whereas the remaining cold part may still form stars (see the NB-TSPH models of Merlin & Chiosi 2006, 2007; Merlin et al. 2012, for more details) so that some residual star formation may always be present, the analysis could also be extended to include this case. However, doing so would not add very much to the present discussion.

The comparison between the Renzini & Peng (2015) relation and our age grid sheds light on two important features. First, the mean SFR vs mass relationship (red dashed line) crosses the rest-frame tracks of the models at values of the ages that vary with the mass: this can be seen by looking, for each mass, at the point of the age grid nearest to the dark red dashed line. On this basis, our simple model shows that objects belonging to the group of “star-forming galaxies” are not coeval. In ad-

dition, the dark red dashed line crosses each rest-frame curve at an age which increases with increasing mass: shortly speaking, on average greater stellar masses are associated with older galaxies. This argument, in addition to the need of bursts and mergers to explain colors of cluster galaxies, leads to enforce the idea that galaxies as stellar assemblies are further older systems. Secondly, the slopes of the theoretical SFR vs stellar-mass relationship are practically identical to that of the [Renzini & Peng \(2015\)](#) relation. This is a reminiscence of the result found in [Chiosi et al. \(2017\)](#) (their Fig. 11, top panel) with same model galaxies but a slightly different cosmological approach. All this, confirms that, in spite of its complexity and caveats, our model does a good job in placing galaxies inside a physically sounded cosmological context.

In conclusion, we can briefly say that both the distribution of galaxies on the CMD and the SFR vs stellar mass relationship are not straightforward results because they actually stem from the contributions of several different physical properties of galaxy formation and evolution.

6. FINAL REMARKS AND PERSPECTIVES FOR FUTURE STUDIES

We have investigated the CMD of cluster galaxies by exploring the phenomena that could affect the intensity and color of the light they emit: these can be bursts and/or mergers inducing rejuvenation of the stellar component and chemical enrichment, or galactic winds of internal origin or gas removal by external causes both stripping a galaxy of its gas and initiating passive evolution of this latter. All these phenomena are more likely to occur in galaxy clusters than in the field. We have analyzed the impact of these two different physical processes on the evolution by means of two approaches, i.e. galaxy-sized SSPs and realistic chemo-photometric models of galaxies. Among the main results of our study, we recall the following ones:

1) Simulations of bursts of star formation based on SSP-galaxies show the effect of a younger stellar component of arbitrary age, metallicity and mass on the light emitted by an assembly of coeval stars with different age, metallicity and mass. On the $M_V - (B - V)$ plane, adding a younger component leads the host galaxy to shift leftwards and downwards, i.e. towards higher V luminosities and bluer $B - V$ colors: the shift has an amplitude increasing with the mass of the stars engaged in the burst with respect to the mass of the host galaxy and the difference between the mean ages of the two components. Masses and ages are the dominant parameters, the metallicity plays a secondary role. The net effect of random bursts is to broaden the Red Sequence at $z = 0$ making it to stretch down to the reddest part of the Green Valley. Roughly speaking, bursts younger than 3 Gyr already account for more than 60% of the width of the Green Valley.

2) To further test the dispersion inside CMDs engendered by age differences among the underlying stellar populations, we present the simulations of single mergers, which at a first glance provide a much more effective scatter than similarly massive bursts. This is due to the fact that mergers involve a broader mix of ages, i.e. the more massive galaxy in the merger episode may not necessarily be the older one, together with a broader mix of metallicities. The merger simulations present a rich Red Sequence, which slope nicely matches the observational one, and a well crowded Green Valley. Finally, they also partially populate the Blue Cloud, thus suggesting that fractions of young stellar populations larger than allowed by typical bursts are needed.

3) Basing on the CMDs for mergers of SSP-galaxies, we heuristically demonstrated that mergers between galaxies cannot occur independently of the age and mass of the interacting galaxies. Were this the case, mergers would populate regions of the CMD that are seen void of objects. The region in question is the triangle with basis $-20 > M_V > -25$ and height $0.2 < B - V < 0.9$ (see the left panel of Fig. 7), which we named *zone of avoidance*. In other words, not all values of age and mass for the merging galaxies are permitted. The avoidance zone is simply telling the following: *the probability that a galaxy can merge with another of similar mass decreases at increasing the galaxy mass and hence, in the hierarchical scheme, the age*. As matter of facts, only a merger (burst) involving less than about ten percent of the total star mass may leave a post-merger (burst) descendant similar to the progenitor object. The reddest and brightest objects of the Red Sequence crowd in a rather compact group and have no blue counterparts of the same luminosity. This means that they have not acquired a significant amount of mass in a recent time and by virtue of their own color they have remained the same since long time. Therefore, the red bright objects are preferentially made of old stars. The goal has been achieved by introducing a filter (named funnel) for masses and ages of the merging galaxies. The same filter allows us to account for the galaxies crowding the Green Valley in a coherent fashion. Later the filter has been identified with the HGF of the cosmological building up of galaxies.

4) Spurred by the results obtained with SSPs, we turned to galaxy models nicely simulating the collapse of BM into the gravitational potential well of DM, including star formation and chemical enrichment, energy feedback from various sources, and the effect of this in modulating the SFR and triggering galactic winds. We coupled them with a set of HGFs, in turn obtained from their respective HMFs (i.e. [Warren et al. 2006](#); [Angulo et al. 2012](#); [Behroozi et al. 2013](#)), in order to assign random formation redshifts. In this context, we showed that a great deal of the information carried by the precision cosmology is lost when analyzing the integrated properties of galaxies, so that any of the three

HMFs used in this work provides qualitatively the same results. We exploited the HGFs to build up our samples of synthetic galaxies, the demography of which has been validated by comparison with the most massive galaxy cluster in the ILLUSTRIS-1 simulation.

5) We have set up three groups of galaxy models, namely the early-type galaxies with sudden global galactic wind (ET_{gw}) and those with star formation modulated by the feedback energy injection and continuous galactic winds that remove part of the gas without stopping star formation (ET_{ms}), and late-type galaxies (LT_{ms}). With aid of these models we have repeated the merger simulations by applying the HGF as the cosmological funnel to assign ages and masses to galaxies. The results of this experiments mainly recover those with SSP-galaxies, however the major difference that a more prominent and adequate occupation of the three loci is at work. Again a simply tuned approach.

6) The simulated samples have proven to be solid in explaining CMDs of cluster galaxies, together with the SFR vs stellar mass relationship which is also related to the light emitted by stars. Although with some caveats regarding the crudeness of our approach (e.g. only one merger per galaxy is allowed), we can conclude that our model provides consistent insights on phenomena

at work during the formation and evolution histories of galaxies.

7) Finally, we would like to note that despite the many drawbacks and limitations our simple tool for describing the population of galaxies in a cluster is able to get the essence of a number of physical phenomena shaping the CMDs of cluster galaxies. The present approach is not meant to replace full cosmological simulations but simply to play an ancillary role in testing many physical assumptions and ingredients before they are incorporated in heavy numerical simulations.

ACKNOWLEDGMENTS

We would like to thank the anonymous referee for the many constructive remarks and suggestions that greatly helped us to improve the content and layout of the paper. M.S. thanks Giulia Despali, Chiara Mancini and Alessia Moretti for helpful discussions and hints. C.C. would like to thank Rosaria Tantalo and Emanuela Chiosi for valuable collaboration, and the Department of Physics and Astronomy of the Padua University for the friendly hospitality and computational support. The tool HMFcalc and the public data from the ILLUSTRIS-project have been amply used in this study.

REFERENCES

- Adami C., Mazure A., Biviano A., Katgert P., Rhee G., 1998, *A&A*, 331, 493
- Angulo R. E., Springel V., White S. D. M., Jenkins A., Baugh C. M., Frenk C. S., 2012, *MNRAS*, 426, 2046
- Aragon-Salamanca A., Ellis R. S., Couch W. J., Carter D., 1993, *MNRAS*, 262, 764
- Arimoto N., Yoshii Y., 1987, *A&A*, 173, 23
- Baade W., 1944, *ApJ*, 100, 137
- Baldry I. K., Glazebrook K., Brinkmann J., Ivezić Ž., Lupton R. H., Nichol R. C., Szalay A. S., 2004, *ApJ*, 600, 681
- Barai P. et al., 2013, *MNRAS*, 430, 3213
- Bartelmann M., 2010, *Classical and Quantum Gravity*, 27, 233001
- Baum W. A., 1959, *PASP*, 71, 106
- Behroozi P. S., Wechsler R. H., Wu H.-Y., Busha M. T., Klypin A. A., Primack J. R., 2013, *ApJ*, 763, 18
- Bell E. F. et al., 2004, *ApJ*, 608, 752
- Bertelli G., Girardi L., Marigo P., Nasi E., 2008, *A&A*, 484, 815
- Bertelli G., Nasi E., Girardi L., Marigo P., 2009, *A&A*, 508, 355
- Blaauw A., 1959, in *IAU Symposium, Vol. 10, The Hertzsprung-Russell Diagram*, Greenstein J. L., ed., p. 105
- Blanton M. R. et al., 2003, *AJ*, 125, 2348
- Bond J. R., Cole S., Efstathiou G., Kaiser N., 1991, *ApJ*, 379, 440
- Boselli A., Gavazzi G., 2014, *A&A Rv*, 22, 74
- Bothwell M. S., Maiolino R., Kennicutt R., Cresci G., Mannucci F., Marconi A., Ciccone C., 2013, *MNRAS*, 433, 1425
- Bower R. G., Benson A. J., Malbon R., Helly J. C., Frenk C. S., Baugh C. M., Cole S., Lacey C. G., 2006, *MNRAS*, 370, 645
- Bower R. G., Lucey J. R., Ellis R. S., 1992a, *MNRAS*, 254, 601
- Bower R. G., Lucey J. R., Ellis R. S., 1992b, *MNRAS*, 254, 601
- Bower R. G., Lucey J. R., Ellis R. S., 1992c, *MNRAS*, 254, 589
- Boylan-Kolchin M., Springel V., White S. D. M., Jenkins A., Lemson G., 2009, *MNRAS*, 398, 1150
- Bressan A., Chiosi C., Fagotto F., 1994, *ApJS*, 94, 63
- Burstein D., Bender R., Faber S., Nolthenius R., 1997, *AJ*, 114, 1365
- Burstein D., Bender R., Faber S. M., Nolthenius R., 1995, *Astrophysical Letters and Communications*, 31, 95
- Butcher H., Oemler, Jr. A., 1978, *ApJ*, 219, 18
- Buzzoni A., 2002, *AJ*, 123, 1188

- Cantiello M., Blakeslee J. P., 2007, *ApJ*, 669, 982
- Cardelli J. A., Clayton G. C., Mathis J. S., 1989, *ApJ*, 345, 245
- Cariddi S., D’Onofrio M., Fasano G., Poggianti B. M., Moretti A., Gullieuszik M., Bettoni D., Sciarratta M., 2018, *A&A*, 609, A133
- Cassarà L. P. et al., 2016, *A&A*, 593, A9
- Cassarà L. P., Piovan L., Chiosi C., 2015, *MNRAS*, 450, 2231
- Cassarà L. P., Piovan L., Weiss A., Salaris M., Chiosi C., 2013, *MNRAS*, 436, 2824
- Cava A. et al., 2009, *A&A*, 495, 707
- Chabrier G., Hennebelle P., Charlot S., 2014, *ApJ*, 796, 75
- Chester C., Roberts M. S., 1964, *AJ*, 69, 635
- Chiosi C., 1967, *Mem. Soc. Astron. Italiana*, 38, 3
- Chiosi C., 1980, *A&A*, 83, 206
- Chiosi C., 2002, in *Astronomical Society of the Pacific Conference Series*, Vol. 253, *Chemical Enrichment of Intracluster and Intergalactic Medium*, Fusco-Femiano R., Matteucci F., eds., p. 285
- Chiosi C., 2007, in *Astronomical Society of the Pacific Conference Series*, Vol. 374, *From Stars to Galaxies: Building the Pieces to Build Up the Universe*, Vallenari A., Tantalò R., Portinari L., Moretti A., eds., p. 439
- Chiosi C., Bertelli G., Bressan A., 1988, *A&A*, 196, 84
- Chiosi C., Bressan A., Portinari L., Tantalò R., 1998, *A&A*, 339, 355
- Chiosi C., Carraro G., 2002, *MNRAS*, 335, 335
- Chiosi C., Merlin E., Piovan L., 2012, *ArXiv e-prints*
- Chiosi C., Merlin E., Piovan L., Tantalò R., 2014, *Galaxies*, 2, 300
- Chiosi C., Sciarratta M., D’Onofrio M., Chiosi E., Brotto F., De Michele R., Politino V., 2017, *ApJ*, 851, 44
- Chua K. T. E., Pillepich A., Rodríguez-Gomez V., Vogelsberger M., Bird S., Hernquist L., 2017, *Monthly Notices of the Royal Astronomical Society*, 472, 4343
- Conroy C., 2013, *ARA&A*, 51, 393
- Conroy C., Graves G. J., van Dokkum P. G., 2014, *ApJ*, 780, 33
- Corwin, Jr. H. G., Buta R. J., de Vaucouleurs G., 1994, *AJ*, 108, 2128
- Cresci G., Mannucci F., Sommariva V., Maiolino R., Marconi A., Brusa M., 2012, *MNRAS*, 421, 262
- Dahmer-Hahn L. G., Riffel R., Rodríguez-Ardila A., Martins L. P., Kehrig C., Heckman T. M., Pastoriza M. G., Dametto N. Z., 2018, *MNRAS*
- Davies R. D., Lewis B. M., 1973, *MNRAS*, 165, 231
- De Lucia G., Blaizot J., 2007, *MNRAS*, 375, 2
- De Lucia G., Springel V., White S. D. M., Croton D., Kauffmann G., 2006, *MNRAS*, 366, 499
- de Vaucouleurs G., 1961, *ApJS*, 5, 233
- de Vaucouleurs G., de Vaucouleurs A., Corwin, Jr. H. G., Buta R. J., Paturel G., Fouqué P., 1991, *Third Reference Catalogue of Bright Galaxies. Volume I: Explanations and references. Volume II: Data for galaxies between 0^h and 12^h. Volume III: Data for galaxies between 12^h and 24^h.*
- Despali G., Vegetti S., 2017, *MNRAS*, 469, 1997
- Dolag K., Jubelgas M., Springel V., Borgani S., Rasia E., 2004, *ApJL*, 606, L97
- Draine B. T., Lee H. M., 1984, *ApJ*, 285, 89
- Dressler A., 1980, *ApJ*, 236, 351
- Dressler A., 1984, *ApJ*, 281, 512
- Faber S. M., 1977, in *Evolution of Galaxies and Stellar Populations*, Tinsley B. M., Larson D. Campbell R. B. G., eds., p. 157
- Faber S. M., Gallagher J. S., 1979, *ARA&A*, 17, 135
- Fan L., Lapi A., Bressan A., Bernardi M., De Zotti G., Danese L., 2010, *ApJ*, 718, 1460
- Fasano G. et al., 2006, *A&A*, 445, 805
- Fasano G. et al., 2012, *MNRAS*, 420, 926
- Fritz J. et al., 2007, *A&A*, 470, 137
- Fritz J. et al., 2011, *A&A*, 526
- Fu X., Bressan A., Marigo P., Girardi L., Montalbán J., Chen Y., Nanni A., 2018, *MNRAS*, 476, 496
- Gallazzi A., Charlot S., Brinchmann J., White S. D. M., 2006, *MNRAS*, 370, 1106
- Gibson B. K., Matteucci F., 1997, *MNRAS*, 291, L8
- Girardi L., Bertelli G., Bressan A., Chiosi C., Groenewegen M. A. T., Marigo P., Salasnich B., Weiss A., 2002, *A&A*, 391, 195
- Gladders M. D., López-Cruz O., Yee H. K. C., Kodama T., 1998, *ApJ*, 501, 571
- Gott, III J. R., Gunn J. E., 1971, *ApJL*, 169, L13
- Guiderdoni B., Rocca-Volmerange B., 1987, *A&A*, 186, 1
- Gullieuszik M. et al., 2015, *A&A*, 581, A41
- Guo Q. et al., 2011, *MNRAS*, 413, 101
- Head J. T. C. G., Lucey J. R., Hudson M. J., Smith R. J., 2014, *MNRAS*, 440, 1690
- Heitmann K., Lukić Z., Habib S., Ricker P. M., 2006, *ApJL*, 642, L85
- Henriques B. M. B., White S. D. M., Thomas P. A., Angulo R., Guo Q., Lemson G., Springel V., Overzier R., 2015, *MNRAS*, 451, 2663
- Hernquist L., Springel V., 2003, *MNRAS*, 341, 1253
- Hertzsprung E., 1909, *Astronomische Nachrichten*, 179, 373
- Jiang F., vandenBosch F. C., 2016, *Monthly Notices of the Royal Astronomical Society*, 458, 2848
- Kaiser N., 1984, *ApJL*, 284, L9

- Katsianis A., Tescari E., Blanc G., Sargent M., 2017, *MNRAS*, 464, 4977
- Kauffmann G., 1996, *MNRAS*, 281, 487
- Kauffmann G., Charlot S., 1998, 297, L23+
- Kennicutt, Jr. R. C., 1983, *AJ*, 88, 483
- Kodama T., Arimoto N., 1997, *A&A*, 320, 41
- Kodama T., Arimoto N., Barger A. J., Aragón-Salamanca A., 1998, *A&A*, 334, 99
- Kodama T., Bower R. G., Bell E. F., 1999, *MNRAS*, 306, 561
- Komatsu E. et al., 2011, *ApJS*, 192, 18
- Kravtsov A. V., Borgani S., 2012, *ARA&A*, 50, 353
- Kroupa P., 2008, in *Astronomical Society of the Pacific Conference Series*, Vol. 390, *Pathways Through an Eclectic Universe*, Knappen J. H., Mahoney T. J., Vazdekis A., eds., p. 3
- Lacey C., Cole S., 1993, *MNRAS*, 262, 627
- Larson R. B., 1974, *MNRAS*, 169, 229
- Lee J. H., Oh S., Jeong H., Yi S. K., Kyeong J., Park B.-G., 2017, *ApJ*, 844, 81
- Lintott C. J. et al., 2008, *MNRAS*, 389, 1179
- López-Cruz O., Barkhouse W. A., Yee H. K. C., 2004, *ApJ*, 614, 679
- Lukić Z., Heitmann K., Habib S., Bashinsky S., Ricker P. M., 2007, *ApJ*, 671, 1160
- Madau P., Dickinson M., 2014, *ARA&A*, 52, 415
- Maio U., Dolag K., Ciardi B., Tornatore L., 2007, *MNRAS*, 379, 963
- Mannucci F., Cresci G., 2012, *Memorie della Societa Astronomica Italiana Supplementi*, 19, 214
- Mannucci F., Cresci G., Maiolino R., Marconi A., Gnerucci A., 2010, *MNRAS*, 408, 2115
- Masters K. L. et al., 2010, *MNRAS*, 405, 783
- Matsuoka K., Nagao T., Marconi A., Maiolino R., Mannucci F., Cresci G., Terao K., Ikeda H., 2018, *A&A*, 616, L4
- Mei S. et al., 2009, *ApJ*, 690, 42
- Menci N., Fontana A., Giallongo E., Salimbeni S., 2005, *ApJ*, 632, 49
- Menci N., Rosati P., Gobat R., Strazzullo V., Rettura A., Mei S., Demarco R., 2008, *ApJ*, 685, 863
- Merlin E., Chiosi C., 2006, 457, 437
- Merlin E., Chiosi C., 2007, 473, 733
- Merlin E., Chiosi C., Piován L., Grassi T., Buonomo U., La Barbera F., 2012, *MNRAS*, 427, 1530
- Merritt D., 1988, in *The Minnesota lectures on Clusters of Galaxies and Large-Scale Structure*, Dickey J. M., ed., Vol. 5, pp. 175–196
- Moretti A. et al., 2017, *A&A*, 599, A81
- Moster B. P., Naab T., White S. D. M., 2013, *MNRAS*, 428, 3121
- Murray S. G., Power C., Robotham A. S. G., 2013, *Astronomy and Computing*, 3, 23
- Nelson D. et al., 2015, *Astronomy and Computing*, 13, 12
- Nelson D. et al., 2018, *MNRAS*, 475, 624
- Pahre M. A., Djorgovski S. G., de Carvalho R. R., 1996, *ApJL*, 456, L79
- Pasha I., Kriek M., Johnson B., Conroy C., 2018, in *American Astronomical Society Meeting Abstracts*, Vol. 231, *American Astronomical Society Meeting Abstracts* 231, p. 149.29
- Peebles P. J. E., 2002, in *Astronomical Society of the Pacific Conference Series*, Vol. 283, *A New Era in Cosmology*, Metcalfe N., Shanks T., eds., p. 351
- Pillepich A. et al., 2017, *ArXiv e-prints*
- Piovan L., Chiosi C., Merlin E., Grassi T., Tantaló R., Buonomo U., Cassarà L. P., 2011a, *ArXiv e-prints*
- Piovan L., Chiosi C., Merlin E., Grassi T., Tantaló R., Buonomo U., Cassarà L. P., 2011b, *ArXiv e-prints*
- Piovan L., Chiosi C., Merlin E., Grassi T., Tantaló R., Buonomo U., Cassarà L. P., 2011c, *ArXiv e-prints*
- Piovan L., Tantaló R., Chiosi C., 2006a, *MNRAS*, 366, 923
- Piovan L., Tantaló R., Chiosi C., 2006b, *MNRAS*, 370, 1454
- Planelles S., Borgani S., Dolag K., Ettori S., Fabjan D., Murante G., Tornatore L., 2013, *MNRAS*, 431, 1487
- Portinari L., Chiosi C., Bressan A., 1998, *A&A*, 334, 505
- Press W. H., Schechter P., 1974, *ApJ*, 187, 425
- Puchwein E., Springel V., 2013, *MNRAS*, 428, 2966
- Rasera Y., Teyssier R., 2006, *A&A*, 445, 1
- Renzini A., Peng Y.-j., 2015, *ApJL*, 801, L29
- Richstone D., 1990, in *Clusters of Galaxies*, Oegerle W. R., Fitchett J., Danly L., eds., p. 231
- Roediger J. C. et al., 2017, *ApJ*, 836, 120
- Russell H. N., 1914, *Popular Astronomy*, 22, 275
- Salaris M., Weiss A., Cassarà L. P., Piován L., Chiosi C., 2014, *A&A*, 565, A9
- Salasnich B., Girardi L., Weiss A., Chiosi C., 2000, *A&A*, 361, 1023
- Salpeter E. E., 1955, 121, 161
- Sandage A., 1957, *ApJ*, 125, 435
- Sandage A., 1972, *ApJ*, 176, 21
- Sandage A., Visvanathan N., 1978a, *ApJ*, 225, 742
- Sandage A., Visvanathan N., 1978b, *ApJ*, 223, 707
- Schade D., Carlberg R. G., Yee H. K. C., López-Cruz O., Ellingson E., 1996, *ApJ*, 464, L63
- Schaye J. et al., 2015, *MNRAS*, 446, 521
- Schmidt M., 1959, *ApJ*, 129, 243
- Sheth R. K., Tormen G., 2002, *MNRAS*, 329, 61
- Silk J., Mamon G. A., 2012, *Research in Astronomy and Astrophysics*, 12, 917
- Springel V., 2005, *MNRAS*, 364, 1105

- Springel V., Di Matteo T., Hernquist L., 2005, MNRAS, 361, 776
- Springel V., Hernquist L., 2003a, MNRAS, 339, 289
- Springel V., Hernquist L., 2003b, MNRAS, 339, 312
- Stanford S. A., Eisenhardt P. R., Dickinson M., 1998, ApJ, 492, 461
- Stott J. P., Pimblet K. A., Edge A. C., Smith G. P., Wardlow J. L., 2009, MNRAS, 394, 2098
- Sunyaev R. A., Zeldovich Y. B., 1972, A&A, 20, 189
- Tantalo R., 2005, in ASSL Vol. 327: The Initial Mass Function 50 Years Later, Corbelli E., Palla F., Zinnecker H., eds., pp. 235–+
- Tantalo R., Chinellato S., Merlin E., Piovan L., Chiosi C., 2010, A&A, 518, A43
- Tantalo R., Chiosi C., Bressan A., Fagotto F., 1996, A&A, 311, 361
- Tantalo R., Chiosi C., Bressan A., Marigo P., Portinari L., 1998, A&A, 335, 823
- Terlevich A. I., Caldwell N., Bower R. G., 2001, MNRAS, 326, 1547
- Tinker J., Kravtsov A. V., Klypin A., Abazajian K., Warren M., Yepes G., Gottlöber S., Holz D. E., 2008, ApJ, 688, 709
- Tinsley B. M., 1968, 151, 547
- Tinsley B. M., 1980, FCPH, 5, 287
- Tornatore L., Borgani S., Dolag K., Matteucci F., 2007, MNRAS, 382, 1050
- Torrey P., Vogelsberger M., Genel S., Sijacki D., Springel V., Hernquist L., 2014, MNRAS, 438, 1985
- Torrey P. et al., 2017, ArXiv e-prints
- Tran K.-V. H., Franx M., Illingworth G. D., van Dokkum P., Kelson D. D., Blakeslee J. P., Postman M., 2007, ApJ, 661, 750
- Tremonti C. A. et al., 2004, ApJ, 613, 898
- Tully R. B., Mould J. R., Aaronson M., 1982, ApJ, 257, 527
- Valentinuzzi T. et al., 2011, A&A, 536, A34
- van den Bergh S., 1976, ApJ, 206, 883
- van Dokkum P. G., Franx M., Kelson D. D., Illingworth G. D., Fisher D., Fabricant D., 1998, ApJ, 500, 714
- Varela J. et al., 2009, A&A, 497, 667
- Visvanathan N., Sandage A., 1977, ApJ, 216, 214
- Vogelsberger M. et al., 2014, MNRAS, 444, 1518
- Vogelsberger M., Sijacki D., Kereš D., Springel V., Hernquist L., 2012, MNRAS, 425, 3024
- Warren M. S., Abazajian K., Holz D. E., Teodoro L., 2006, ApJ, 646, 881
- White S. D. M., Frenk C. S., 1991, ApJ, 379, 52
- Wiersma R. P. C., Schaye J., Smith B. D., 2009a, MNRAS, 393, 99
- Wiersma R. P. C., Schaye J., Theuns T., Dalla Vecchia C., Tornatore L., 2009b, MNRAS, 399, 574
- Wong O. I. et al., 2012, MNRAS, 420, 1684

APPENDIX

A. MAGNITUDES AND COLORS OF SSPS

Table 6 provides a short summary of magnitudes and colors in the Johnson-Bessell-Brett photometric system for SSPs with solar composition (metallicity $Z = 0.019$), a few selected values of the age, and three popular IMFs, namely Chabrier et al. (2014), Kroupa (2008), and Salpeter (1955), and references therein. The SSPs are from the library calculated by Tantalo (2005). It is evident that while the magnitudes depend on the adopted IMF, the colors are much less affected, so that passing from one IMF to another could be detected only with very accurate photometry. Ages are in years.

Table 6. The first column is the logarithm of the age in years.

log(Age)	V	BOL	BC	U-B	B-V	V-R	R-I	V-J	V-H	V-K	V-L	V-M	V-N
CHABRIER													
7.00	4.935	3.228	-1.707	-0.632	0.216	0.269	0.326	1.222	1.811	1.888	1.973	1.797	1.993
8.00	6.658	5.987	-0.671	-0.267	0.133	0.172	0.224	0.861	1.358	1.422	1.485	1.347	1.494
9.00	8.476	8.074	-0.402	0.194	0.546	0.363	0.419	1.687	2.393	2.536	2.620	2.515	2.613
9.50	9.686	9.049	-0.638	0.407	0.867	0.539	0.567	2.104	2.866	2.996	3.086	2.953	3.084
10.00	10.851	10.061	-0.789	0.625	0.991	0.595	0.604	2.236	3.010	3.143	3.234	3.103	3.232
10.15	11.181	10.282	-0.899	0.702	1.030	0.616	0.623	2.308	3.092	3.229	3.322	3.193	3.320
KROUPA													
7.00	0.261	-1.425	-1.686	-0.620	0.200	0.256	0.314	1.181	1.761	1.837	1.922	1.748	1.942
8.00	1.735	1.091	-0.644	-0.255	0.128	0.163	0.212	0.816	1.294	1.357	1.418	1.286	1.426
9.00	3.238	2.869	-0.368	0.183	0.537	0.356	0.407	1.627	2.312	2.450	2.533	2.430	2.527
9.50	4.251	3.638	-0.613	0.393	0.856	0.533	0.558	2.067	2.820	2.948	3.037	2.906	3.035
10.00	5.231	4.452	-0.779	0.624	0.989	0.595	0.603	2.226	2.995	3.127	3.218	3.089	3.217
10.15	5.527	4.633	-0.893	0.705	1.031	0.618	0.623	2.304	3.086	3.222	3.315	3.188	3.314
SALPETER													
7.00	-0.705	-2.388	-1.683	-0.619	0.253	0.291	0.346	1.285	1.881	1.959	2.045	1.869	2.066
8.00	1.238	0.571	-0.668	-0.264	0.137	0.175	0.227	0.872	1.370	1.435	1.499	1.362	1.506
9.00	3.010	2.614	-0.396	0.192	0.546	0.364	0.419	1.676	2.375	2.517	2.601	2.498	2.594
9.50	4.138	3.506	-0.633	0.406	0.866	0.541	0.568	2.097	2.853	2.983	3.074	2.944	3.070
10.00	5.189	4.398	-0.791	0.634	0.997	0.602	0.613	2.245	3.010	3.145	3.238	3.114	3.232
10.15	5.479	4.581	-0.899	0.714	1.038	0.626	0.633	2.319	3.095	3.233	3.328	3.208	3.322

B. HGFS AND CMD SIMULATIONS FOR CLUSTER GALAXIES

In this section first we provide the coefficients of the 4-th order interpolating polynomials of eqn. (23) that are used to derive the HGFs as a function of the redshift, with the resulting galaxy populations expected at redshift $z = 0$ in clusters of typical size visible in Table 4. The coefficients are listed in Tables from 7 to 9. The clusters radii under consideration and total number of galaxies per cluster are given in Table 4, finally the associated CMDs are shown in Fig. 14. For the sake of simplicity, the CMDs are for galaxy models with no galactic winds. See the main text for more details on the subject.

Table 7. Coefficients of the polynomial interpolation of [Warren et al. \(2006\)](#) HGF.

$\log M (M_{\odot} h^{-1})$	A ₄	A ₃	A ₂	A ₁	A ₀
7	2.00391e-05	-0.00069	-0.00172	0.06186	2.75945
8	1.96696e-05	-0.00064	-0.00597	0.07659	2.50057
9	1.68349e-05	-0.00048	-0.01349	0.09530	1.57895
10	1.05238e-05	-0.00019	-0.02622	0.11542	0.67160
11	-5.80424e-07	0.00031	-0.04848	0.13077	-0.21784
12	-1.90090e-05	0.00113	-0.09057	0.12322	-1.09097
13	-4.46934e-05	0.00218	-0.17571	0.04452	-2.21666

Table 8. Coefficients of the polynomial interpolation of [Angulo et al. \(2012\)](#) HGF.

$\log M (M_{\odot} h^{-1})$	A ₄	A ₃	A ₂	A ₁	A ₀
7	2.32293e-05	-0.00090	0.00198	0.02171	2.87802
8	2.77379e-05	-0.00103	-0.00076	0.03137	2.60891
9	3.11068e-05	-0.00110	-0.00692	0.04606	1.67251
10	3.03550e-05	-0.00098	-0.01955	0.06583	0.74492
11	2.19534e-05	-0.00054	-0.04451	0.08647	-0.17097
12	-8.06725e-07	0.00049	-0.09497	0.08979	-1.07614
13	-3.75088e-05	0.00197	-0.19783	0.01701	-2.23637

Table 9. Coefficients of the polynomial interpolation of [Behroozi et al. \(2013\)](#) HGF.

$\log M (M_{\odot} h^{-1})$	A ₄	A ₃	A ₂	A ₁	A ₀
7	2.16291e-05	-0.00070	-0.00221	0.04123	2.78376
8	2.09428e-05	-0.00064	-0.00643	0.05307	2.52830
9	1.93874e-05	-0.00054	-0.01316	0.06578	1.61067
10	1.68678e-05	-0.00039	-0.02392	0.07592	0.70708
11	1.34064e-05	-0.00019	-0.04253	0.07624	-0.18019
12	7.44482e-06	0.00016	-0.07894	0.04842	-1.05531
13	-2.09921e-06	0.00059	-0.15666	-0.05354	-2.19023

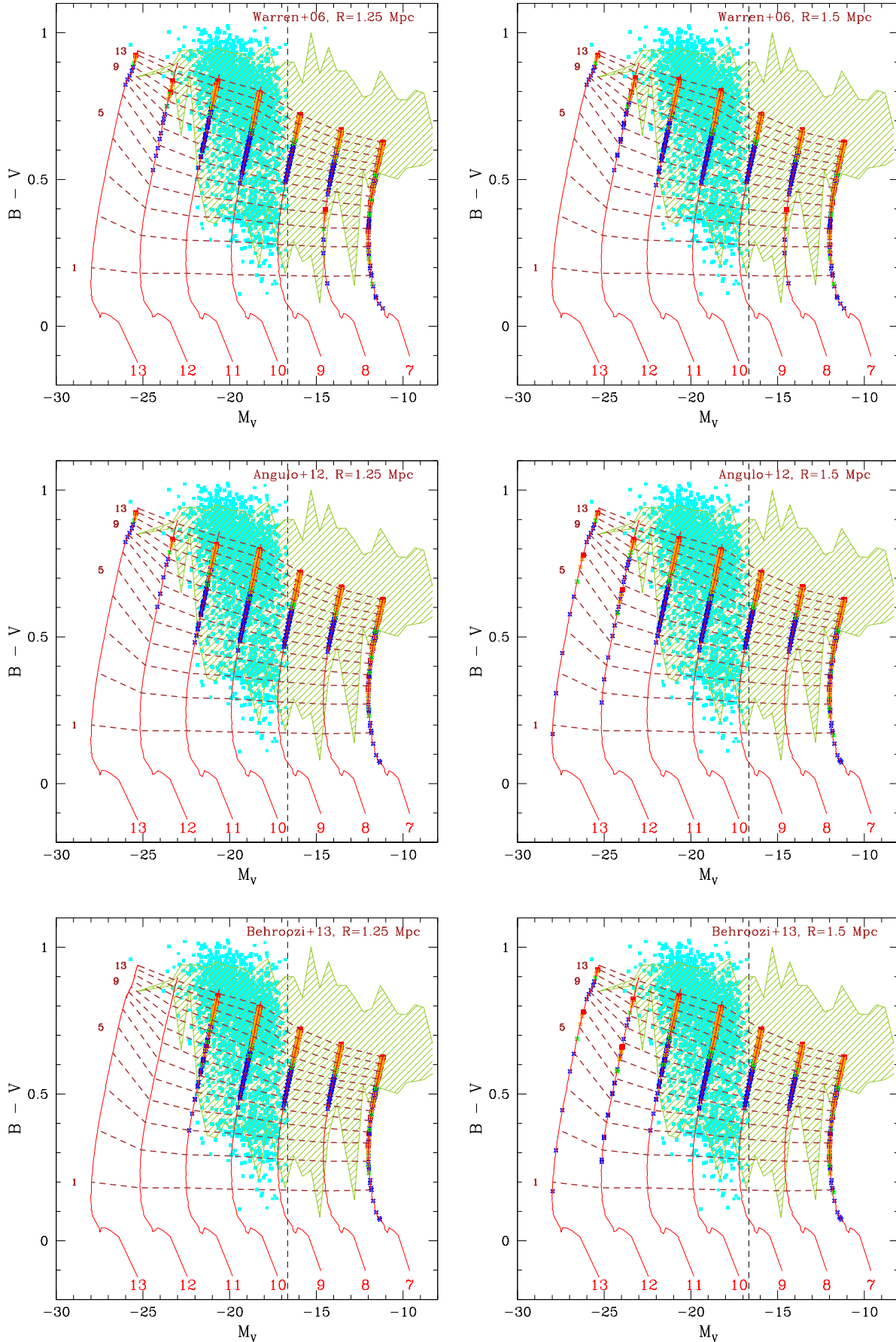


Figure 14. CMDs of all simulated clusters: left panels are for radius 1.25 Mpc, right panels 1.50 Mpc; from top to bottom, Warren et al. (2006), Angulo et al. (2012), Behroozi et al. (2013). Color code and symbols as in Figure 10.